Design of a tetravalent RGD peptide capable of simultaneous binding with multiple integrin αvβ3 for targeted radionuclide therapy

Yuki Mizuno[1,2*], Thanakrit Suebboonprathueng[3], Satoru Onoe[4], Hiromichi Akizawa[4], Ken-ichi Nishijima[5], Kazuhiro Takahashi[5], Yuji Kuge[1,2]

[1] Central Institute of Isotope Science, Hokkaido University, Sapporo 060-0815, Japan

[2] Global Center for Biomedical Science and Engineering, Hokkaido University, Sapporo 060-8638, Japan

[3] Graduate School of Biomedical Science and Engineering, Hokkaido University, Sapporo 060-8638, Japan

[4] Laboratory of Physical Chemistry, Showa Pharmaceutical University, Machida 194-8543, Japan

[5] Advanced Clinical Research Center, Fukushima Medical University, Fukushima 960-1295, Japan

Abstract

For targeted radionuclide therapy, radioligands that exhibit high and persistent tumor uptake are indispensable. We previously synthesized a ^{99m}Tc-labeled hexavalent RGD peptide (^{99m}Tc-(RGD)$_6$) as a tumor imaging agent targeting integrin αvβ3. ^{99m}Tc-(RGD)$_6$ showed high in vivo tumor uptake with long retention due to simultaneous binding to multiple integrin αvβ3 receptors. The purpose of this study was to apply this finding to the design of a multivalent RGD peptide labeled with ^{211}At, a promising α-emitting radionuclide for radionuclide therapy. As a candidate compound, a tetravalent RGD peptide (H_2N-(RGD)$_4$) was synthesized and radiolabeled with ^{125}I, a homologous element of At, for basic studies. As expected, ^{125}I-(RGD)$_4$ retained the capability of simultaneous binding and showed comparable in vivo tumor uptake to ^{99m}Tc-(RGD)$_6$. Finally, ^{211}At-(RGD)$_4$ was synthesized with >95% radiochemical purity and exhibited an almost identical biodistribution pattern to ^{125}I-(RGD)$_4$. These results indicate that ^{211}At-(RGD)$_4$ might be a potential radioligand for integrin αvβ3-targeted radionuclide therapy.

Keywords

Integrin, RGD peptide, Theranostics, Multivalency, Astatine-211

Introduction

Targeted radionuclide therapy has recently received considerable attention, largely due to its clinical success in the treatment of cancer. [1, 2] In contrast to external radiation therapy, targeted radionuclide therapy requires the administration of radiolabeled ligands to patients, with tumor tissue subsequently irradiated by radiation (α, β particles, etc.) emitted from the radiolabeled ligands. Consequently, the therapeutic efficacy of targeted radionuclide therapy strongly depends on the degree of accumulation of radiolabeled ligands in the tumor tissue. [3] Hence, the development of radiolabeled ligands with high uptake and persistent retention in tumor tissues is a prerequisite for the successful implementation of targeted radionuclide therapy.

The multivalent effect has been extensively exploited in the development of such radiolabeled ligands. [4-6] The multivalent effect is a phenomenon in which multivalent ligands possessing multiple copies of targeting ligands display enhanced binding affinity to target molecules in comparison to their monovalent counterparts. [7-9] Furthermore, multivalent ligands that simultaneously bind to multiple target molecules exhibit prolonged retention at the target molecules, a phenomenon known as the "chelate effect".[4, 10] This "chelate effect" has the potential to markedly enhance the therapeutic efficacy of targeted radionuclide therapy by prolonging the residence time of radiolabeled ligands in tumor tissues.

Our group has continued the development of ^{99m}Tc-labeled multivalent cyclic RGD peptides targeting integrin αvβ3 for the diagnosis of cancer. [11-13] Integrin αvβ3 is an attractive target molecule for cancer diagnosis and therapy as its expression is upregulated in various malignant tumors including glioma, [14] breast cancer, [15] and neuroendocrine

cancer. [16] Furthermore, integrin αvβ3 forms clusters responding to the surrounding environment. [17] The formation of clusters is a favorable characteristic for multivalent interaction because the distance between the two adjacent binding pockets becomes shorter and multivalent ligands can form simultaneous multiple bonds more easily. [11] In addition, it was reported that c(RGDfK) had an excellent binding specificity towards integrin αvβ3 over other integrin subtypes such as integrin αvβ5, αvβ6, and αvβ8. [18] Recently, we synthesized a ^{99m}Tc-labeled hexavalent c(RGDfK) peptide that possessed semi-rigid ($_{D}$Pro-Gly)$_6$ as a linker molecule (Figure 1, ^{99m}Tc-(RGD)$_6$) and demonstrated that ^{99m}Tc-(RGD)$_6$ bound to multiple integrin αvβ3 receptors simultaneously, resulting in the enhanced tumor retention in a cell-based experiment. [11] Consistent with the in vitro result, ^{99m}Tc-(RGD)$_6$ showed high tumor uptake with long retention in tumor-bearing nude mice. Thus, the chemical structure of ^{99m}Tc-(RGD)$_6$ represents an excellent template for the design of novel radioligands for integrin αvβ3 targeted radionuclide therapy.

The selection of radionuclides is another important factor for successful radionuclide therapy. Recent clinical studies have indicated that α-emitting radionuclides may be a viable alternative to β^--emitting radionuclides in cases where treatment resistance is a concern. [19, 20] However, ^{99m}Tc in ^{99m}Tc-(RGD)$_6$ cannot be replaced with medically relevant α emitting radionuclides, such as ^{225}Ac or ^{212}Pb, due to the unique coordination property of isocyanide ligands to metal ions. [21] Accordingly, to apply the chemical structure of ^{99m}Tc-(RGD)$_6$ for effective radionuclide therapy, at least one of the six RGD peptides in ^{99m}Tc-(RGD)$_6$ has to be replaced with a functional group that can be used for radiolabeling reactions with α-emitting radionuclides.

Therefore, in this study, we aimed to design and synthesize multivalent RGD peptides that have the following two properties: 1) the capability of simultaneous binding to

multiple integrin αvβ3 receptors, and 2) having a functional group that can be used for labeling reactions with α-emitting radionuclides. To achieve this goal, we first examined what substructures of ^{99m}Tc-(RGD)$_6$ were essential for simultaneous binding to integrin αvβ3 receptors, in other words, to what extent RGD peptide truncation could be tolerated without impairing the capability of simultaneous binding. Because it turned out that ^{99m}Tc-(RGD)$_4$ (Figure 1) retained the capability of simultaneous binding, we designed and synthesized a tetravalent RGD peptide that has a free amine for radiolabeling reactions (Figure 1, H_2N-(RGD)$_4$). This tetravalent RGD peptide was radiolabeled with ^{125}I for basic studies, and its tumor uptake properties were evaluated both in vitro and in vivo. Finally, the tetravalent RGD peptide was also radiolabeled with ^{211}At, a promising α-emitting radionuclide for cancer therapy, and its biodistribution was evaluated in tumor-bearing nude mice.

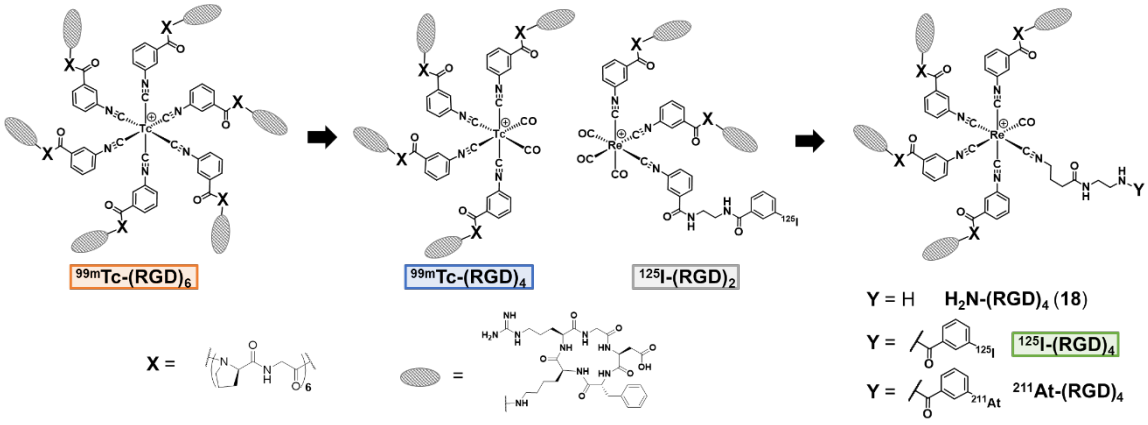

Figure 1. Chemical structures of radiolabeled multivalent RGD peptide tested in this study. Only ^{125}I-(RGD)$_2$ does not possess a *trans*-positioned RGD peptide combination.

Results

Synthesis of *cis*-[^{99m}Tc][Tc^{I}(CO)$_2$(L1)$_4$]$^+$ (^{99m}Tc-(RGD)$_4$). The synthesis scheme of *cis*-[^{99m}Tc][Tc^{I}(CO)$_2$(L1)$_4$]$^+$ (^{99m}Tc-(RGD)$_4$) is shown in Scheme 1. *fac*-[^{99m}Tc][Tc^{I}(CO)$_3$(OH$_2$)$_3$]$^+$ was prepared as an intermediate with >95% radiochemical purity and reacted with L1 (Scheme 1) at 95°C for 30 min. Upon the heating, L1 coordinated to Tc^{I} by replacing the three water molecules and one CO molecule in *fac*-[^{99m}Tc][Tc^{I}(CO)$_3$(OH$_2$)$_3$]$^+$ to generate *cis*-[^{99m}Tc][Tc^{I}(CO)$_2$(L1)$_4$]$^+$. The replacement of one CO molecule in [^{99m}Tc][Tc^{I}(CO)$_3$]$^+$ with isocyanide ligands has been reported by several groups. [13, 22, 23] Theoretically, [^{99m}Tc][Tc^{I}(CO)$_2$(L1)$_4$]$^+$ can have two isomers, *cis*- and *trans*-[^{99m}Tc][Tc^{I}(CO)$_2$(L1)$_4$]$^+$. However, the formation of *trans*-[^{99m}Tc][Tc^{I}(CO)$_2$(L1)$_4$]$^+$ is unlikely because CO prefers to be *trans* to σ-donating ligands such as isocyanide ligands to maximize its π-accepting ability. [24] An *ab initio* MO study also demonstrated the instability of *trans*-[Tc(CO)$_2$(H$_2$O)$_4$]$^+$ over *cis*-[Tc(CO)$_2$(H$_2$O)$_4$]$^+$. [25] To the best of our knowledge, the formation of *trans*-[Tc/Re(CO)$_2$(L)$_4$]$^+$ has never been reported. After HPLC purification, *cis*-[^{99m}Tc][Tc^{I}(CO)$_2$(L1)$_4$]$^+$ was obtained with >95% radiochemical purity (Figure S1). Its molar activity was as high as that of [^{99m}Tc]Tc^{VII}O$_4^-$ (≈ 2 GBq/nmol depending on the elution interval) since the unlabeled ligand was removed by the HPLC purification. On the other hand, because we collected only the HPLC eluent near the peak top to increase the radiochemical purity (Figure S2), the non-decay corrected radiochemical yield was 25 ± 1% (n = 4). Its nonradioactive rhenium counterpart, *cis*-[$^{185/187}$Re][Re^{I}(CO)$_2$(L1)$_4$]CF$_3$CO$_2$ (**5**), was synthesized according to Scheme 2 and registered a similar retention time to that of *cis*-[^{99m}Tc][Tc(CO)$_2$(L1)$_4$]$^+$ in HPLC analysis (Figure S2). Given that our previous study showed very high stability of

cis-[^{99m}Tc][Tc(CO)$_2$(CN-GABA-GlyGly-c(RGDfK))$_4$]$^+$ in mouse plasma, [13] it can be anticipated that *cis*-[^{99m}Tc][Tc(CO)$_2$(L1)$_4$]$^+$ will exhibit a comparably high level of stability.

Scheme 1. Synthesis scheme of *cis*-[^{99m}Tc][Tc(CO)$_2$(L1)$_4$]$^+$ (**^{99m}Tc-(RGD)$_4$**)[a]

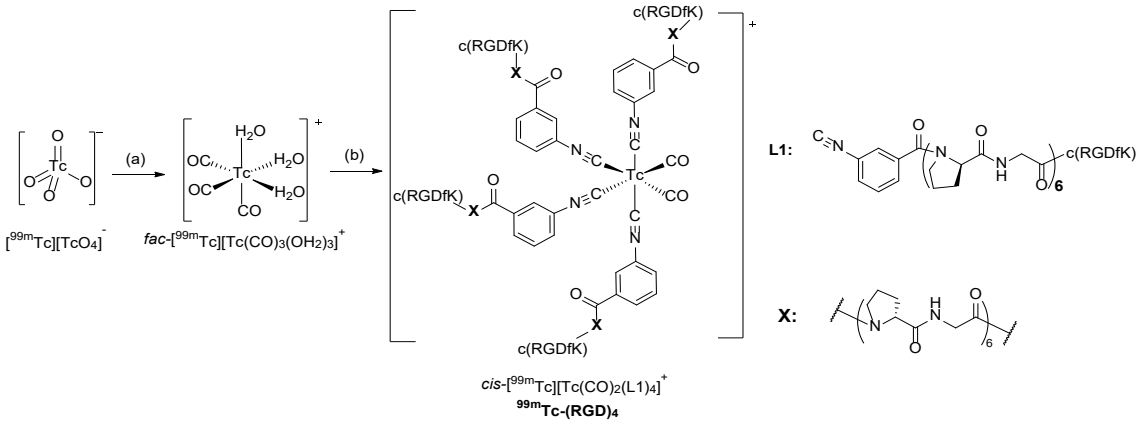

[a]Reagents and conditions: (a) CO, $NaBH_4$, Na_2CO_3, Sodium (+)-tartrate dihydrate; (b) L1, 0.2 M MES buffer (pH 5.0).

Scheme 2. Synthesis scheme of *cis*-[$^{185/187}$Re][Re(CO)$_2$(L1)$_4$]CF$_3$CO$_2$ (**Re-(RGD)$_4$**) (**5**)[a]

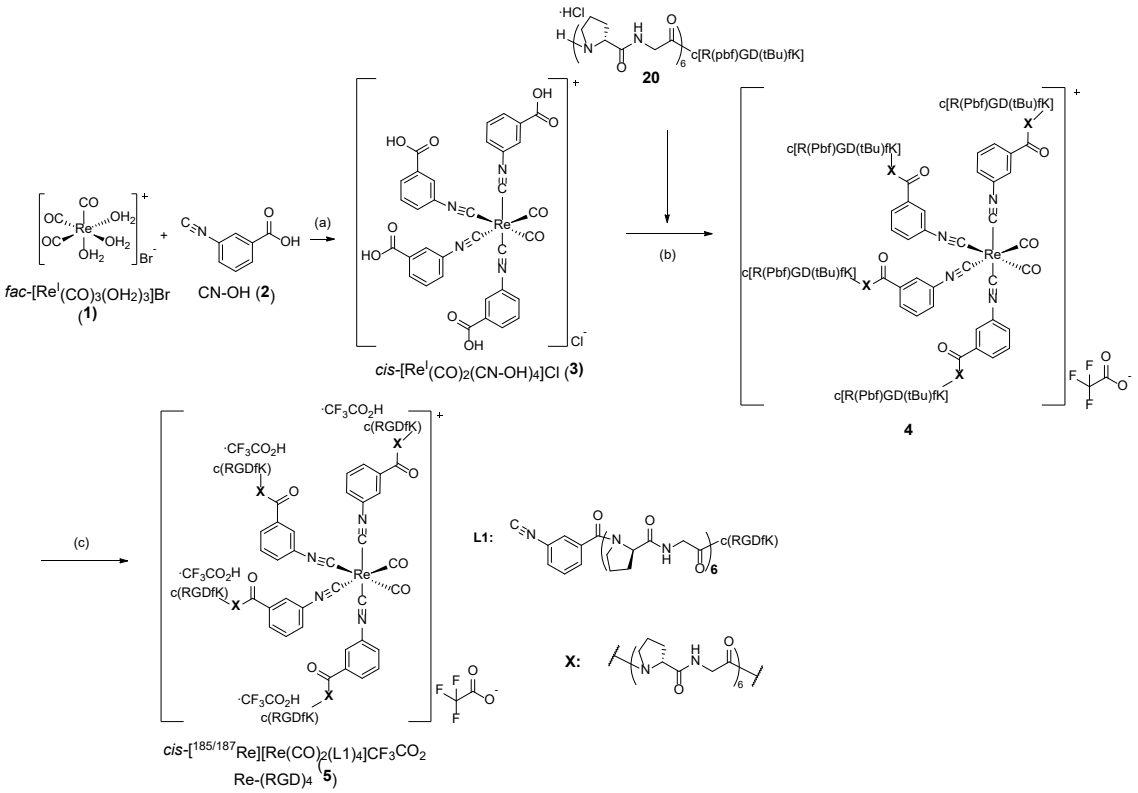

[a]Reagents and conditions: (a) 0.1 M P.B. (pH 8.0), 20%; (b) WSCD·HCl, HOBt·H$_2$O, DMF; (c) TFA/TIS/Water, 17% over steps b–c.

Synthesis of ^{125}I-(RGD)$_2$. The synthesis scheme of ^{125}I-(RGD)$_2$ is shown in Scheme 3. We first synthesized *fac*-[Re^{I}(CO)$_3$(CN-OH)$_3$]Cl (**6**), and its chemical structure was verified by ESI-MS and IR. The IR spectrum showed two CO peaks, indicating its *facial* configuration.[26] In the next reaction, one of the three carboxylic acids in compound **6** was condensed with *N*-Boc-ethylenediamine to provide compound **7**. The remaining two carboxylic acids in compound **7** were then condensed with H-(pG)$_6$-c[R(pbf)GD(tBu)fK] (**20**) to provide compound **8**. Compound **8** was then fully deprotected by TFA and reacted with [^{125}I]SIB to provide ^{125}I-(RGD)$_2$. After HPLC purification, ^{125}I-(RGD)$_2$ was obtained with a radiochemical yield of 25 ± 10% (n = 3) and a radiochemical purity of > 95%. Its

molar activity was as high as that of [^{125}I]NaI (carrier-free, 644 GBq/mg, 82.2 MBq/nmol) since unreacted compound **9** was removed by the HPLC purification. On the other hand, the reaction between compound **9** and [^{nat}I]SIB provided multiple peaks and only yielded a trace amount of ^{nat}I-(RGD)$_2$ (**12**) (Data not shown). Thus, ^{nat}I-(RGD)$_2$ (**12**) was synthesized according to Scheme 4. ^{nat}I-(RGD)$_2$ (**12**) and ^{125}I-(RGD)$_2$ registered a similar retention time in an HPLC analysis (Figure S3). Considering our previous report that exhibited high metabolic stability of [^{99m}Tc][Tc(CO)$_3$(CN-βAla-GlyGly-c(RGDfK)$_3$)]$^+$ in mouse plasma, [27] it is reasonable to assume that ^{125}I-(RGD)$_2$, a similar tris(isocyanide)rhenium complex, will also have similarly high stability.

Scheme 3. Synthesis scheme of ^{125}**I-(RGD)$_2$**[a]

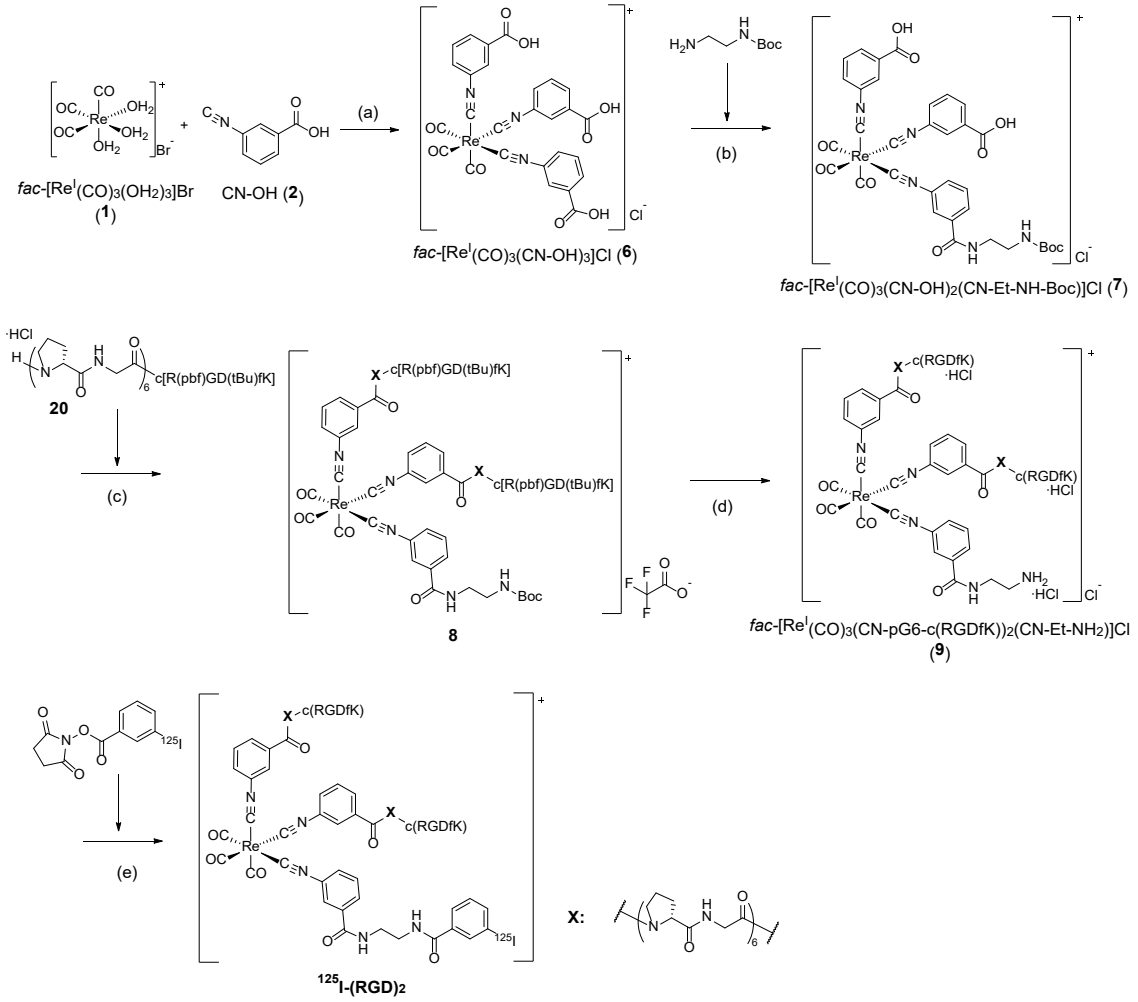

[a]Reagents and conditions: (a) 0.1 M A.B. (pH 6.0), 67%; (b) WSCD·HCl, HOBt·H_2O, DMF, 25%; (c) WSCD·HCl, HOBt·H_2O, DIPEA, DMF; (d) TFA/TIS/Water, 0.01 M HCl, 15% over steps c–d; (e) [^{125}I]SIB, 0.1 M borate buffer (pH 9.0).

Scheme 4. Synthesis scheme of ^{nat}**I-(RGD)$_2$ (12)**[a]

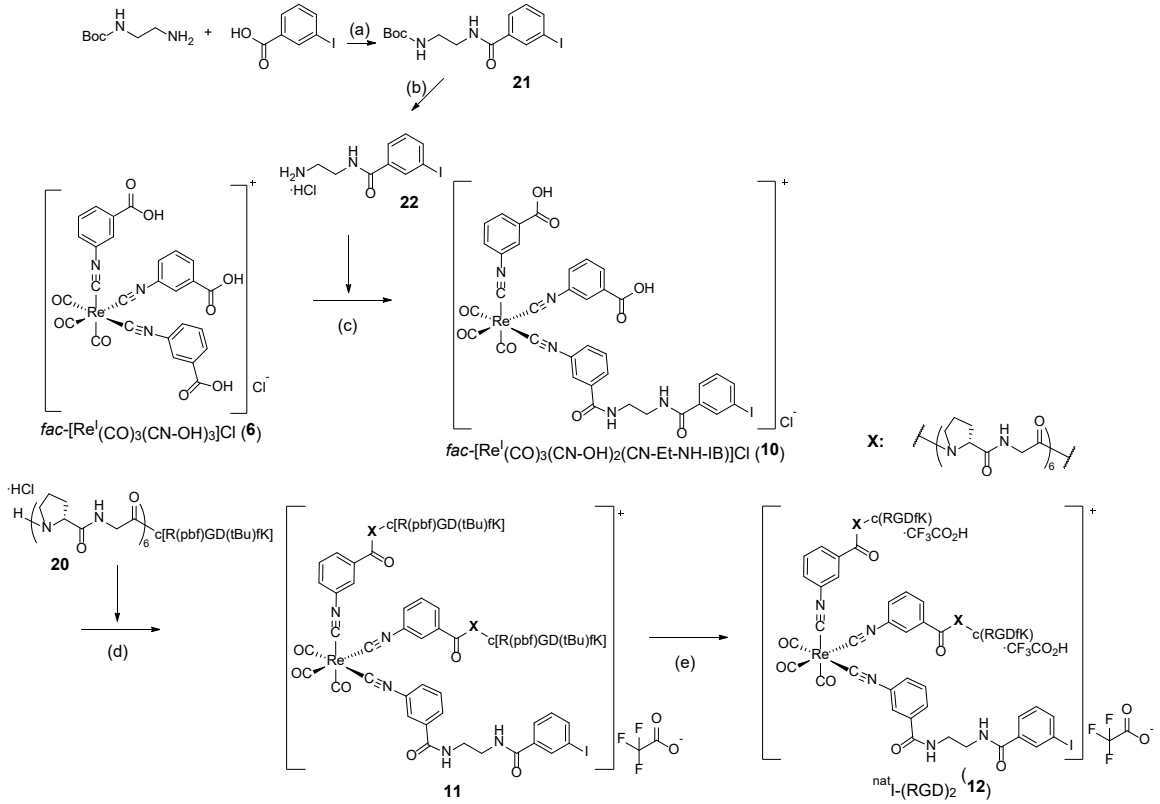

[a]Reagents and conditions: (a) WSCD·HCl, $CHCl_3$, 64%; (b) 4 M HCl/1,4-dioxane, 89%; (c) WSCD·HCl, HOBt·H_2O, DIPEA, DMF, 12%; (d) WSCD·HCl, HOBt·H_2O, DIPEA, DMF; (e) TFA/TIS/Water, 38% over steps d–e.

Synthesis of ^{125}I-(RGD)$_4$. The synthesis scheme of ^{125}I-(RGD)$_4$ is shown in Scheme 5. First, we synthesized [Re^{I}(CN-OMe)$_4$(CO)Br] (**14**) from the reaction between [Re^{I}(CO)$_5$Br] and CN-OMe (**13**) according to a method reported by Claude et al. [28] In their report, the selective formation of *trans*-[Re^{I}(CN-R)$_4$(CO)Br] over *cis*-[Re^{I}(CN-R)$_4$(CO)Br] was observed. On the other hand, our ^{1}H NMR analysis indicated the formation of both *trans*-[Re^{I}(CN-OMe)$_4$(CO)Br] and *cis*-[Re^{I}(CN-OMe)$_4$(CO)Br] (Figure S12). This difference may have arisen from the different σ-donating and/or π-accepting ability of the isocyanide ligands employed. At this step, these two isomers were not separated and used as a mixture in the next reaction. In Scheme 4 reaction (c), Br in [Re^{I}(CN-OMe)$_4$(CO)Br] (**14**) was removed by the addition of $AgPF_6$, followed by the coordination of CN-GABA-Et-NH-Boc (**24**) to Re^{I}. After HPLC purification, *cis*-[Re^{I}(CN-OMe)$_4$(CO)(CN-GABA-Et-NH-Boc)]CF_3CO_2 (**15a**) and *trans*-[Re^{I}(CN-OMe)$_4$(CO)(CN-GABA-Et-NH-Boc)]CF_3CO_2 (**15b**) were isolated. These two isomers were easily distinguished by the different patterns of methoxy peaks in their ^{1}H NMR analyses. Since all methoxy groups in **15b** are equivalent due to its high symmetry, a single methoxy peak (3.955 ppm) was observed in the ^{1}H NMR of **15b** (Figure S14). On the other hand, two different methoxy peaks (3.950 and 3.955 ppm) were observed in the ^{1}H NMR of **15a** due to its lower symmetry (Figure S13).

We used **15a** in the flowing experiments because the configuration of isocyanide coordinations in **15a** (Scheme 5) was identical to that in ^{99m}Tc-(RGD)$_4$ (Scheme 1). After removing methyl ester in *cis*-[Re^{I}(CN-OMe)$_4$(CO)(CN-GABA-Et-NH-Boc)]CF_3CO_2 (**15a**) using NaOH, *cis*-[Re^{I}(CN-OH)$_4$(CO)(CN-GABA-Et-NH-Boc)] (**16**) was condensed with 4 equivalent of H-(pG)$_6$-c[R(pbf)GD(tBu)fK] (**20**) to provide compound **17**. Compound **17** was then fully deprotected by TFA and reacted with [^{125}I]SIB to provide

^{125}I-(RGD)$_4$. Its non-radioactive iodine counterpart (**19**) registered a similar retention time to that of ^{125}I-(RGD)$_4$ in HPLC analysis (Figure S4). The radiochemical yield of ^{125}I-(RGD)$_4$ was 57.5% (n = 2), and the radiochemical purity was > 95%. As in the case of ^{125}I-(RGD)$_2$, the molar activity of ^{125}I-(RGD)$_4$ was 82.2 MBq/nmol.

Synthesis of ^{211}At-(RGD)$_4$. The synthesis scheme of ^{211}At-(RGD)$_4$ was the same as that of ^{125}I-(RGD)$_4$, except for the final step. At the final step, [^{211}At]SAB was reacted with H_2N-(RGD)$_4$ (**18**) to provide ^{211}At-(RGD)$_4$. [^{211}At]SAB was prepared as an intermediate with a non-decay corrected radiochemical yield of 60 ± 12% (n = 4). In the final reaction step (reaction (h), Scheme 5), because around 50% of the radioactivity was stuck in the plastic reaction vessel, 58 ± 21% (n = 3) of the initial radioactivity was subjected to HPLC purification. After HPLC purification, methanol in the purified solution was removed by rotary evaporation. However, again, around half of the radioactivity was stuck in the glass round bottom flask, and 50 ± 10% (n = 3) of the radioactivity was recovered to the solution. As a result, the overall radiochemical yield (non-decay corrected) of the final step was 20 ± 8% (n = 3). Nevertheless, the radiochemical purity after the HPLC purification was >95%, and its non-radioactive iodine counterpart (**19**) registered a similar retention time to that of ^{211}At-(RGD)$_4$ in HPLC analysis (Figure S5). Because H_2N-(RGD)$_4$ could be removed by HPLC purification, the molar activity of ^{211}At-(RGD)$_4$ was the same as the maximum theoretical molar activity of ^{211}At, 16.2 GBq/nmol.

Scheme 5. Synthesis scheme of ^{125}**I-(RGD)$_4$ and ^{211}At-(RGD)$_4$**[a]

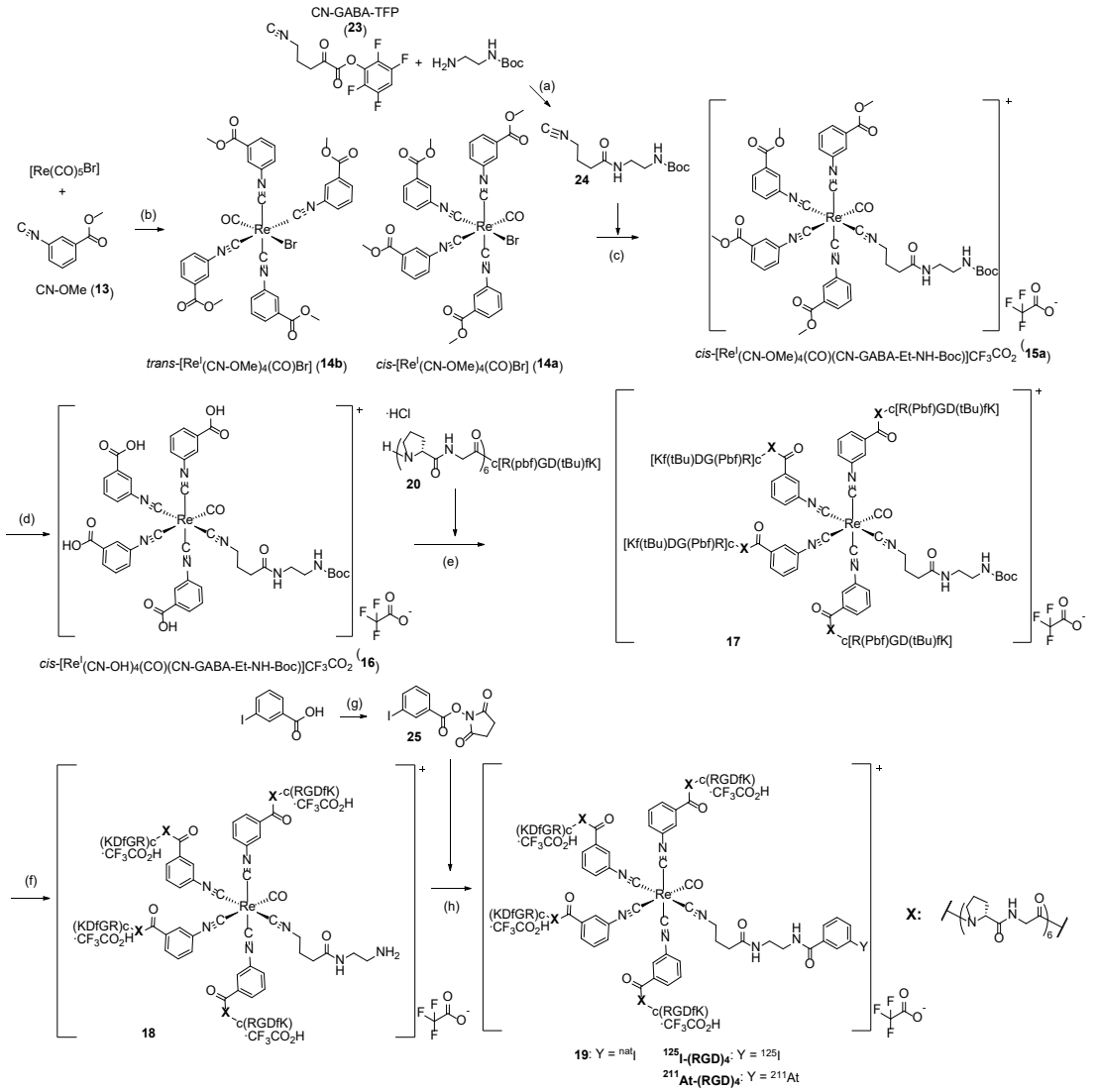

[a]Reagents and conditions: (a) $NaHCO_3$, DMF, 35% (b) Toluene, 13%; (c) $AgPF_6$, $CHCl_3$, MeOH, 29%; (d) 1.0 M NaOH, MeOH, quant.; (e) HATU, DIPEA, DMF; (f) TFA/TIS/Water, 67% over steps e–f; (g) N-hydroxysuccinimide, WSCD·HCl, dichloromethane, 81%; (h) [^{nat}I]SIB (25), [^{125}I]SIB, or [^{211}At]SAB, 0.1 M borate buffer (pH 9.0).

In vitro stability of ^{125}I-(RGD)$_4$. The stability of ^{125}I-(RGD)$_4$ was evaluated in mouse plasma. Before HPLC analysis, plasma proteins were precipitated by the addition of ethanol. The recovery rate of the radioactivity to the supernatant solution was > 96%. The intact ratio determined by HPLC analysis after 1 h and 24 h incubation was 96.1 ± 0.1% and 95.2 ± 0.9%, respectively (Figure S6), indicating the excellent metabolic stability of ^{125}I-(RGD)$_4$ in biological conditions.

In vitro binding affinity to integrin αvβ3. The integrin αvβ3 binding affinity of Re-(RGD)$_6$, Re-(RGD)$_4$ (**5**), ^{nat}I-(RGD)$_4$ (**19**), and ^{nat}I-(RGD)$_2$ (**12**) were determined by displacement of [^{125}I]c[RGDy(3-I)V] bound to U87MG cells. The IC$_{50}$ values are summarized in Table 1. The IC$_{50}$ values showed a tendency to decrease as the number of RGD peptide increased. Re-(RGD)$_6$ showed the lowest, and ^{nat}I-(RGD)$_2$ showed the highest IC$_{50}$ value, while Re-(RGD)$_4$ and ^{nat}I-(RGD)$_4$ showed similar IC$_{50}$ values.

Table 1. The IC$_{50}$ value of each compound

Compound	IC$_{50}$, nM	95% C.I. [a]
Re-(RGD)$_6$	2.49	1.94-3.18
Re-(RGD)$_4$ (**5**)	10.7	6.99-16.2
^{nat}I-(RGD)$_4$ (**19**)	13.1	9.53-18.2
^{nat}I-(RGD)$_2$ (**12**)	40.8	25.1-65.1

[a]C.I. = confidence interval

Cellular uptake and dissociation study. The cellular uptakes of ^{99m}Tc-(RGD)$_6$, ^{99m}Tc-(RGD)$_4$, ^{125}I-(RGD)$_4$, and ^{125}I-(RGD)$_2$ after 2 h incubation at 37°C were evaluated using U87MG and MDA-MB-435S cells as integrin αvβ3 positive cell lines. The expression of integrin β3 in these two cell lines was confirmed separately by western blotting analyses (Figure S7). In both cell lines, the uptake value followed the order of ^{99m}Tc-(RGD)$_6$ > ^{99m}Tc-(RGD)$_4$ > ^{125}I-(RGD)$_4$ > ^{125}I-(RGD)$_2$ (Figures 2a and 2b). Coincubation with 50 μM c(RGDyV) significantly reduced the cellular uptakes, indicating that the four radioligands accumulated in the cells in an integrin αvβ3-specific manner. The dissociation kinetics of the four radioligands from U87MG and MDA-MB-435S cells were also evaluated. At first, the four radioligands were incubated with U87MG or MDA-MB-435S cells at 37°C for 2 h, and the cells were washed and incubated in the buffer without radioligands. Percentages of initial specific uptake (see Experimental Section) were determined at 1, 5, 10, and 60 min after the initiation of dissociation. As shown in Figures 2c and 2d, ^{99m}Tc-(RGD)$_6$ showed the slowest, and ^{125}I-(RGD)$_2$ showed the fastest dissociation. ^{99m}Tc-(RGD)$_4$ and ^{125}I-(RGD)$_4$ showed similar dissociation kinetics. The order of dissociation kinetics of the four radioligands did not differ between the two cell lines.

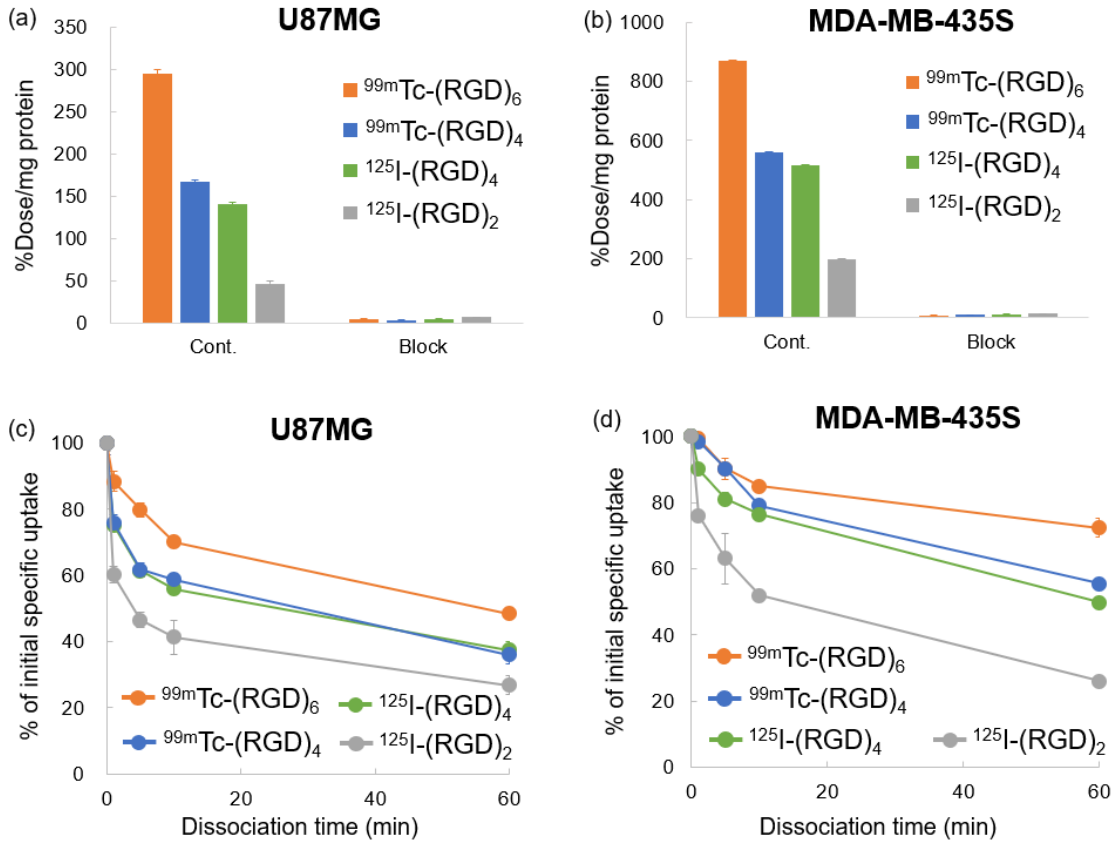

Figure 2. The cellular uptakes of ^{99m}Tc-(RGD)$_6$, ^{99m}Tc-(RGD)$_4$, ^{125}I-(RGD)$_4$, and ^{125}I-(RGD)$_2$ in (a) U87MG cells and (b) MDA-MB-435S cells. The cellular uptake values were determined after incubating the radioligands with cells for 2 h at 37°C. The results are expressed as %Dose/mg protein and mean ± SD (n = 3). Blocking experiments were performed by co-incubation with 50 μM c(RGDyV). The dissociation kinetics of the four radioligands from (c) U87MG cells and (d) MDA-MB-435S cells. The dissociation from cells was measured at 1, 5, 10, and 60 min after the initiation of dissociation. The results are expressed as % of initial specific uptake and mean ± SD (n = 3).

Dissociation kinetics in the presence of c(RGDyV). The dissociation kinetics of ^{99m}Tc-(RGD)$_6$, ^{99m}Tc-(RGD)$_4$, ^{125}I-(RGD)$_4$, and ^{125}I-(RGD)$_2$ in the presence of 50 μM c(RGDyV) were also evaluated because the presence of competitors can affect the dissociation kinetics of multivalent ligands (Figure 3). As shown in Figure 4, the dissociation kinetics of ^{99m}Tc-(RGD)$_6$, ^{99m}Tc-(RGD)$_4$, and ^{125}I-(RGD)$_4$ were accelerated in the presence of c(RGDyV), whereas that of ^{125}I-(RGD)$_2$ did not change. The dissociation rate constants (k_{off}) of the four radioligands were calculated from the results in Figure 4 and are summarized in Table 2. The k_{off} values of ^{99m}Tc-(RGD)$_6$, ^{99m}Tc-(RGD)$_4$, and ^{125}I-(RGD)$_4$ in the presence of c(RGDyV) were significantly higher than their respective values in the absence of c(RGDyV). On the other hand, the k_{off} value of ^{125}I-(RGD)$_2$ did not differ between the two conditions, in the presence or absence of c(RGDyV).

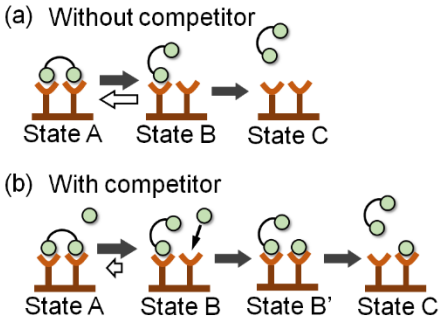

Figure 3. Schematic illustration of multivalent interactions (a) in the absence of competitors and (b) in the presence of competitors. The presence of competitors accelerates the dissociation of multivalent ligands from target molecules when multivalent ligands can simultaneously bind to multiple target molecules. Reprinted with permission from 11. Copyright (2021) American Chemical Society.

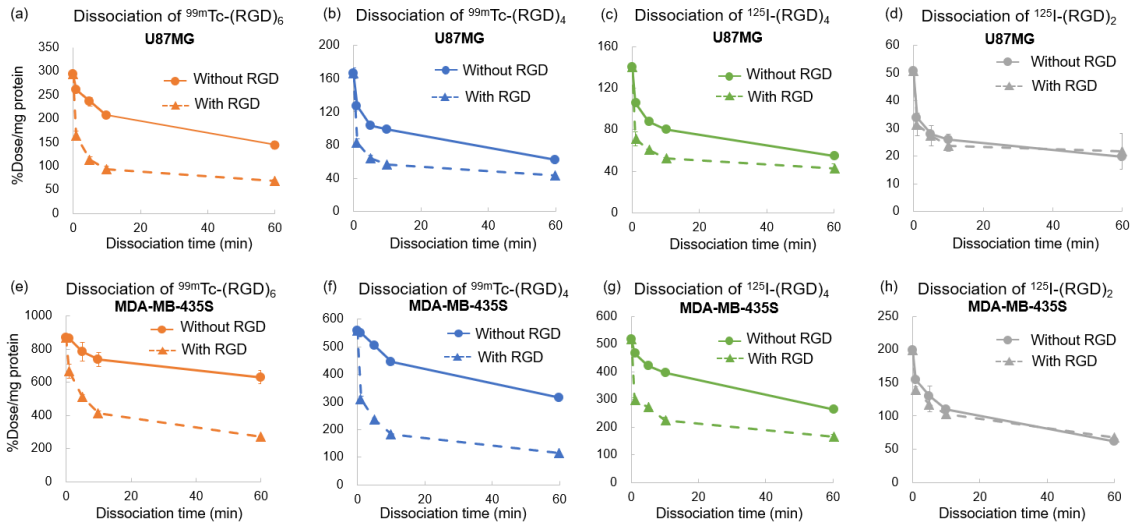

Figure 4. The dissociation kinetics of ^{99m}Tc-(RGD)$_6$, ^{99m}Tc-(RGD)$_4$, ^{125}I-(RGD)$_4$, and ^{125}I-(RGD)$_2$ from (a - d) U87MG cells and (e - h) MDA-MB-435S cells. The results are expressed as %Dose/mg protein and mean ± SD (n = 3). The dissociations were monitored in the presence (With RGD) or absence (Without RGD) of 50 μM c(RGDyV). Only the dissociation of ^{125}I-(RGD)$_2$ did not change between the two conditions.

Table 2. The dissociation rate constants under two different conditions.[a]

Cell line	Compound	without RGD		with RGD		P value[b]
		k_{off} (10^{-2} s^{-1})	R^2	k_{off} (10^{-2} s^{-1})	R^2	
U87MG	^{99m}Tc-$(RGD)_6$	0.14	0.97	1.7	0.97	<0.0001
	^{99m}Tc-$(RGD)_4$	0.23	0.89	2.3	0.97	0.0004
	^{125}I-$(RGD)_4$	0.28	0.91	2.5	0.97	0.0005
	^{125}I-$(RGD)_2$	1.6	0.92	2.2	0.89	0.47
MDA-MB-435S	^{99m}Tc-$(RGD)_6$	0.14	0.89	0.29	0.95	0.045
	^{99m}Tc-$(RGD)_4$	0.098	0.99	1.7	0.94	<0.0001
	^{125}I-$(RGD)_4$	0.11	0.97	2.2	0.92	<0.0001
	^{125}I-$(RGD)_2$	0.19	0.93	0.31	0.88	0.21

[a]The dissociation rate constants were determined by fitting experimental data to a one-phase exponential decay model. [b]Data were compared between "without RGD" and "with RGD" using the extra sum of squares F test in GraphPad Prism v. 9.

Biodistribution. The biodistributions of ^{99m}Tc-(RGD)$_6$, ^{99m}Tc-(RGD)$_4$, ^{125}I-(RGD)$_4$, and ^{125}I-(RGD)$_2$ at 1, 4, and 24 hours post-injection were evaluated using nude mice bearing both U87MG and MDA-MB-435S tumors. The organ uptake values expressed as %ID/g are summarized in Figure 5. ^{125}I-(RGD)$_4$ showed a comparable biodistribution result to ^{99m}Tc-(RGD)$_6$, including U87MG and MDA-MB-435S tumor uptakes. On the other hand, the ^{125}I-(RGD)$_2$ uptakes to U87MG tumor at 4 h and 24 h post-injection were significantly lower than ^{99m}Tc-(RGD)$_6$, ^{99m}Tc-(RGD)$_4$, and ^{125}I-(RGD)$_4$ ($p < 0.05$) (Figure 6a). ^{125}I-(RGD)$_2$ uptake to MDA-MB-435S tumor at 24 h post-injection was significantly lower than ^{99m}Tc-(RGD)$_6$ ($p < 0.05$) (Figure 6b).

The biodistributions of ^{211}At-(RGD)$_4$ and ^{125}I-(RGD)$_4$ at 5 min, 1, 4, and 24 hours post-injection were evaluated using nude mice bearing U87MG tumors. As shown in Figure 7, ^{211}At-(RGD)$_4$ and ^{125}I-(RGD)$_4$ showed almost identical biodistribution patterns with no sign of deastatination and deiodination, as evidenced by their low thyroid and stomach uptakes. In addition, the uptake of ^{211}At-(RGD)$_4$ and ^{125}I-(RGD)$_4$ to U87MG tumor was reduced by >90% by the co-injection of excess c(RGDfK), demonstrating that the U87MG tumor uptakes were integrin αvβ3 specific (Figure S15). Full biodistribution data are described in the supporting information.

Radiation dosimetry estimates of ^{211}At-(RGD)$_4$. The radiation dosimetry estimates of ^{211}At-(RGD)$_4$ in a 25 g mouse phantom model were calculated using the MIRD method. [29] As shown in Table 3, the estimated radiation dose to the U87MG tumor was higher than those of most normal organs. On the other hand, the estimated radiation dose to the kidney was more than 3 times higher than that of the tumor, indicating that the kidney might become a dose-limiting organ when ^{211}At-(RGD)$_4$ is applied for targeted α therapy.

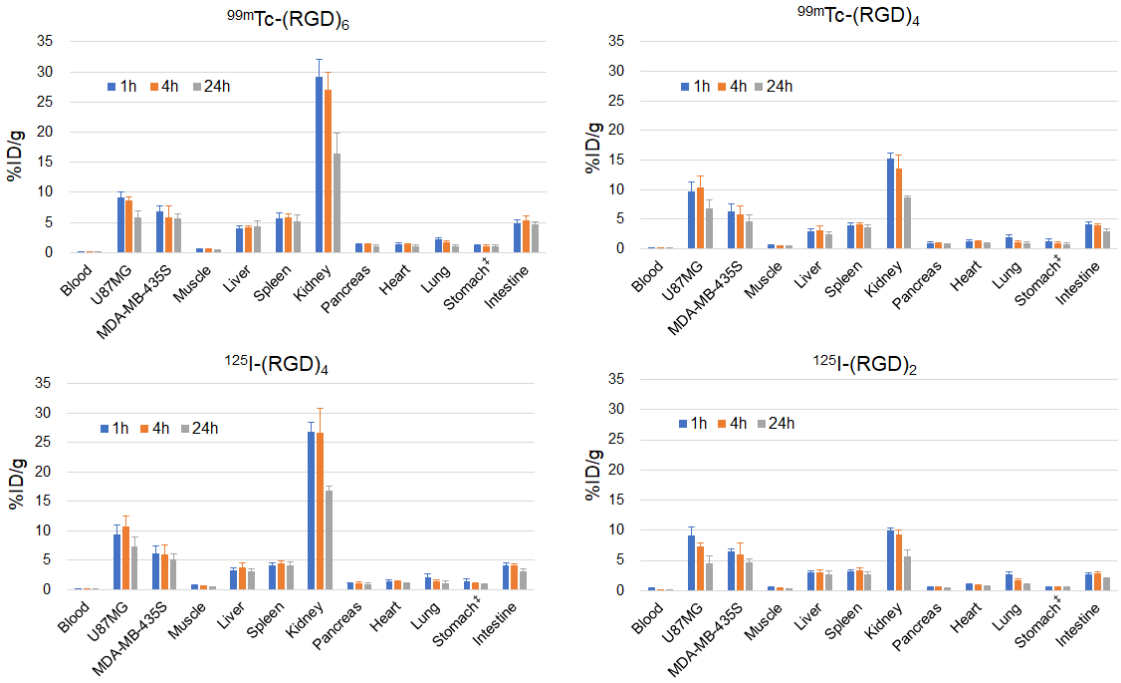

Figure 5. The biodistribution of ^{99m}Tc-(RGD)$_6$, ^{99m}Tc-(RGD)$_4$, ^{125}I-(RGD)$_4$, and ^{125}I-(RGD)$_2$ in nude mice bearing both U87MG and MDA-MB-435S tumors. The results are expressed as %ID/g and mean ± SD (n = 4, 5, or 6). ‡Expressed as %ID.

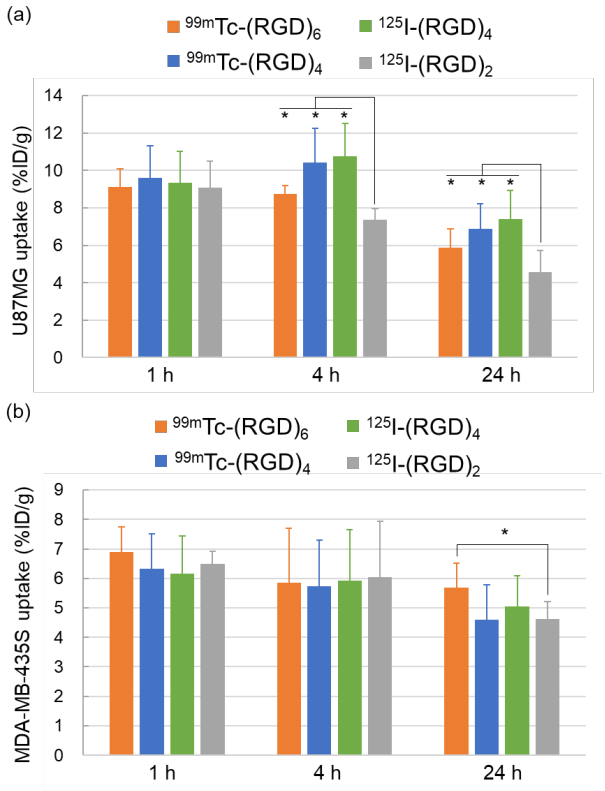

Figure 6. Tumor uptake of ^{99m}Tc-(RGD)$_6$, ^{99m}Tc-(RGD)$_4$, ^{125}I-(RGD)$_4$, and ^{125}I-(RGD)$_2$. (a) U87MG tumor, (b) MDA-MB-435S tumor. The original data is the same as in Figure 5. Statistical analyses between ^{99m}Tc-(RGD)$_6$ and ^{125}I-(RGD)$_2$ and between ^{99m}Tc-(RGD)$_4$ and ^{125}I-(RGD)$_4$ were performed by paired t-test. Statistical analyses between the other combinations were performed by unpaired multiple t-tests with correction for multiple comparisons using the Holm-Sidak method. * $p < 0.05$.

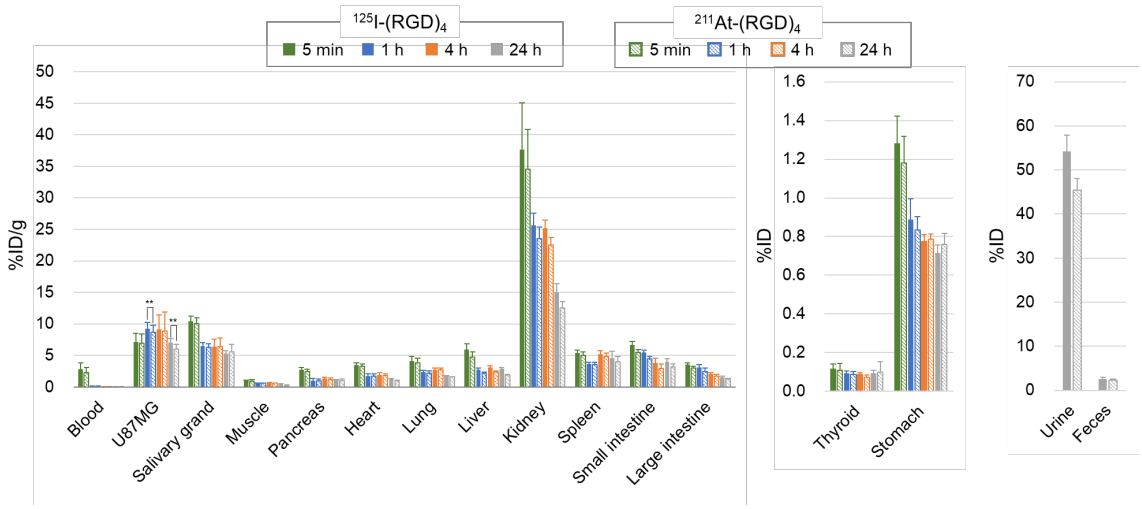

Figure 7. The biodistribution of ^{125}I-(RGD)$_4$ and ^{211}At-(RGD)$_4$ in nude mice bearing U87MG tumors. The results are expressed as %ID/g or %ID and mean ± SD (n = 4). Statistical analyses on the U87MG tumor uptakes were performed by paired t-test. ** $p < 0.01$.

Table 3. Radiation dosimetry estimates of ^{211}At-(RGD)$_4$

	Time-integrated activity coefficient (Bq-h/Bq)	Radiation dosimetry estimates (Gy/MBq)
U87MG Tumor[a]	0.08	1.11
Thyroid	0.01	0.92
Pancreas	0.01	0.07
Heart	0.01	0.09
Lung	0.03	0.50
Liver	0.28	0.23
Kidney	0.79	3.80
Spleen	0.04	0.50
Stomach	0.08	2.15
Small intestine	0.41	0.34
Large intestine	0.12	0.30

[a]The calculation was performed based on the assumption that all tumors had a mass of 0.1 g. A sphere phantom model was used to calculate its radiation dosimetry estimate.

Discussion

The objective of this study was to design and synthesize a novel multivalent RGD peptide that possesses a functional group suitable for labeling reactions with a range of radionuclides and can bind to multiple integrin αvβ3 receptors simultaneously. To achieve this goal, we first truncated the structure of ^{99m}Tc-(RGD)$_6$ to synthesize ^{99m}Tc-(RGD)$_4$ and ^{125}I-(RGD)$_2$ (Figure 1) and evaluated whether these radioligands retain the capability to bind to multiple integrin αvβ3 receptors simultaneously. Given the absence of a non-radioactive technetium isotope, we utilized a non-radioactive rhenium (I) isocyanide complex as a scaffold molecule in ^{125}I-(RGD)$_2$. It has been demonstrated that technetium and rhenium form similar metal isocyanide complexes due to group homology. [21]

To examine whether ^{99m}Tc-(RGD)$_4$ and ^{125}I-(RGD)$_2$ can simultaneously bind to multiple integrin αvβ3 receptors, we evaluated the dissociation kinetics of these radioligands from two integrin αvβ3 positive cell lines (U87MG and MDA-MB-435S cells) in the presence or absence of 50 μM c(RGDyV). It is widely known that the dissociation kinetics of multivalent ligands are accelerated in the presence of competitors when they can simultaneously bind to multiple target molecules. [30-32] As shown in Figure 3, when multivalent ligands bind simultaneously to multiple target molecules, even if one of the bindings dissociates from a target molecule (Figure 3a, State B), the dissociated binding moiety can easily rebind to the target molecule because the entire ligand is still bound to the target. However, when excess competitors exist in the solution, the competitors occupy the vacant binding site (Figure 3b, State B'), and the dissociated moiety cannot rebind to the target molecule. Consequently, the multivalent ligands are readily dissociated from the target molecules. In other words, a change in dissociation

kinetics in the presence of a competitor is a reliable criterion for determining the involvement of simultaneous binding.

As shown in Figure 4 and Table 2, the dissociation kinetics of ^{99m}Tc-(RGD)$_6$ and ^{99m}Tc-(RGD)$_4$ were significantly accelerated in the presence of c(RGDyV), while that of ^{125}I-(RGD)$_2$ did not change. These results demonstrate that ^{99m}Tc-(RGD)$_6$ and ^{99m}Tc-(RGD)$_4$ can simultaneously bind to multiple integrin αvβ3 receptors, whereas ^{125}I-(RGD)$_2$ cannot. Among these three compounds, ^{99m}Tc-(RGD)$_6$ and ^{99m}Tc-(RGD)$_4$ possess both *cis*- and *trans*-positioned RGD peptide combinations, whereas ^{125}I-(RGD)$_2$ has only the *cis*-positioned one. Though we cannot exclude the possibility that the difference in the number of RGD peptides affected the ability of simultaneous binding, the inability of ^{125}I-(RGD)$_2$ to form simultaneous binding may be attributed to the absence of a *trans*-positioned RGD peptide combination. Further investigation is needed to determine whether the *trans* combination is more favorable than the *cis* combination for simultaneous binding.

Based on this result, we designed and synthesized H_2N-(RGD)$_4$ (Figure 1), which has the same stereochemical RGD peptide arrangement as in ^{99m}Tc-(RGD)$_4$ and a free amine that can be used for labeling reactions. As in the case of ^{125}I-(RGD)$_2$, we used a non-radioactive rhenium (I) isocyanide complex as a scaffold molecule in H_2N-(RGD)$_4$. This tetravalent RGD peptide was first radiolabeled with ^{125}I, a radionuclide whose chemical property is similar to ^{211}At due to group homology. For ^{125}I-labeling, [^{125}I]SIB was synthesized as an intermediate and reacted with H_2N-(RGD)$_4$ to provide ^{125}I-(RGD)$_4$. The cellular uptake and retention property of ^{125}I-(RGD)$_4$ was evaluated in the same cell-based experiment as for ^{99m}Tc-(RGD)$_6$, ^{99m}Tc-(RGD)$_4$, and ^{125}I-(RGD)$_2$. As expected, the dissociation kinetics of ^{125}I-(RGD)$_4$ from the integrin αvβ3 positive cell lines were

accelerated in the presence of c(RGDyV), indicating that ^{125}I-(RGD)$_4$ simultaneously bound to multiple integrin αvβ3 receptors on these cell lines (Figure 4). In addition, we attempted to evaluate the internalization rate of ^{125}I-(RGD)$_4$ to U87MG cells using an acid wash technique. However, we found that the cell-remaining radioactivity after washing the cells with an acid buffer (0.2 M Glycine buffer, pH 2.5) was much higher than that after washing with 0.1% BSA binding buffer (Figure S8). This result suggests that the acid washing could not effectively remove the membrane-bound radioactivity. Alternative methods must be explored to accurately evaluate the internalization rate of ^{125}I-(RGD)$_4$.

In this study, we used U87MG and MDA-MB-435S cells as integrin αvβ3 positive cell lines in the cell-based experiment because we speculated that the difference in cell lines might affect the size or density of integrin αvβ3 clusters, thus affecting the capability of radioligands to form simultaneous binding. However, the present results indicate no difference between the two cell lines in whether the four radioligands simultaneously bound to multiple integrin αvβ3 receptors (Figure 4). This result suggests that, at least for U87MG and MDA-MB-435S, the size or density of integrin αvβ3 clusters are similar, and the ability of radioligands to form simultaneous binding is not affected by the difference in cell lines.

Encouraged by the promising in vitro results, we next evaluated the biodistribution of ^{125}I-(RGD)$_4$ in tumor-bearing nude mice and compared the result with that of ^{99m}Tc-(RGD)$_6$, ^{99m}Tc-(RGD)$_4$, and ^{125}I-(RGD)$_2$. ^{125}I-(RGD)$_4$ showed almost identical biodistribution profile as ^{99m}Tc-(RGD)$_6$, including U87MG and MDA-MB-435S tumor uptakes (Figure 5). Importantly, the uptake value of ^{125}I-(RGD)$_4$ in U87MG and MDA-MB-435S tumors at 24 h post-injection was approximately 80% of their respective uptake

value at 1 h post-injection, demonstrating its excellent tumor retention property. These results indicate that H_2N-$(RGD)_4$ may be a promising integrin αvβ3-targeted ligand suitable for radionuclide therapy.

Finally, we radiolabeled H_2N-$(RGD)_4$ with ^{211}At to obtain ^{211}At-$(RGD)_4$. Its synthesis scheme was similar to ^{125}I-$(RGD)_4$. [^{211}At]SAB was synthesized as an intermediate and reacted with H_2N-$(RGD)_4$ to provide ^{211}At-$(RGD)_4$. Though the radiochemical yield was suboptimal, ^{211}At-$(RGD)_4$ was obtained with >95% radiochemical purity. In the biodistribution experiment using U87MG-bearing nude mice, ^{211}At-$(RGD)_4$ displayed an almost identical biodistribution pattern to that of ^{125}I-$(RGD)_4$ (Figure 7), though the tumor uptake of ^{211}At-$(RGD)_4$ was slightly lower than that of ^{125}I-$(RGD)_4$ at 1 h and 24 h post-injection. Furthermore, the uptake of ^{211}At-$(RGD)_4$ to the thyroid and stomach was very low, indicating negligible in vivo deastatination. This result was somewhat surprising considering previous reports that showed significant in vivo deastatination when astatobenzoyl group was used as a ^{211}At-labeling moiety. [33, 34] On the other hand, recent studies indicated that steric hindrance around astatine was crucial for the high stability of ^{211}At-labeling moieties. [35-37] Thus, the negligible in vivo deastatination of ^{211}At-$(RGD)_4$ might be attributed to the high steric hindrance of the tetravalent RGD peptides around the astatobenzoyl group. Above all, the present result suggests that the biodistribution of ^{211}At-$(RGD)_4$ can be precisely predicted by the SPECT imaging using $^{123/125}$I-$(RGD)_4$, enabling the accurate pre-treatment assessment of its therapeutic efficacy. This case exemplifies the fundamental principle of theranostics.

In this study, we conducted in vitro cellular experiments using the four radioligands to predict their in vivo tumor uptake and retention behavior. However, although notable differences were observed between the four radioligands in the in vitro experiment, these

differences were less pronounced in the in vivo experiment. For example, while the in vitro ^{99m}Tc-(RGD)$_6$ uptake in U87MG cells was 6 times higher than ^{125}I-(RGD)$_2$ (Figure 2a), these two radioligands showed almost the same in vivo U87MG tumor uptake at 1 h post-injection (Figure 6a). In addition, the IC_{50} values did not correlate with the in vivo tumor uptakes. Though mechanisms behind this discrepancy remain to be elucidated, it is plausible that the ratio of cluster formation or the degree of internalization of integrin αvβ3 is different between in vitro and in vivo conditions.

On the other hand, consistent with the fastest dissociation kinetics of ^{125}I-(RGD)$_2$ from U87MG cells observed in the in vitro experiment (Figure 2c), the U87MG tumor uptakes of ^{125}I-(RGD)$_2$ at 4 h and 24 h post-injection were significantly lower than the other three radioligands (Figure 6a). Similarly, the MDA-MB-435S tumor uptake of ^{125}I-(RGD)$_2$ at 24 h post-injection was significantly lower than that of ^{99m}Tc-(RGD)$_6$ (Figure 6b), consistent with its faster in vitro dissociation kinetics from MDA-MB-435S cells (Figure 2d). These results suggest that the present in vitro cellular retention experiment might be useful for identifying radioligands that show relatively fast washout from tumor tissue in vivo.

One of the drawbacks of the multivalent ligand design is increased uptake in off-target tissues. It has been observed that the kidney uptake of multivalent peptides increases as the number of peptides increases. [38] Consistent with this previous report, ^{125}I-(RGD)$_4$ showed more than two times higher kidney uptake than ^{125}I-(RGD)$_2$ (Figure 5). On the other hand, the kidney uptake of ^{125}I-(RGD)$_4$ was also higher than that of ^{99m}Tc-(RGD)$_4$ despite the same number of RGD peptides. This result indicates that the number of RGD peptides is not the only factor that determines the kidney uptake, and complex factors such as overall lipophilicity, charge distribution, etc. must be also considered. [39]

Unfortunately, we have not yet determined what factor made the different kidney uptake of ^{125}I-(RGD)$_4$ and ^{99m}Tc-(RGD)$_4$. However, our previous study indicated that employing different lengths of polyethylene glycol as a linker molecule significantly affected the kidney uptake of ^{99m}Tc-labeled hexavalent RGD peptides, [11] suggesting the potential of polyethylene glycol to modify the kidney uptake of multivalent RGD peptides. Similar results were reported from another group. [40] Furthermore, the incorporation of metabolizable linkers[41-43] or co-administration of renal reabsorption inhibitors[44-46] has been also proven effective in reducing kidney uptake without losing tumor uptake. Thus, as a next step, we plan to investigate whether these strategies can reduce the kidney uptake of ^{211}At/^{125}I-(RGD)$_4$.

Conclusion

In this study, we truncated the structure of ^{99m}Tc-(RGD)$_6$ to synthesize ^{99m}Tc-(RGD)$_4$ and ^{125}I-(RGD)$_2$ and demonstrated that ^{99m}Tc-(RGD)$_4$ retained the capability to form simultaneous binding while ^{125}I-(RGD)$_2$ did not. Based on this finding, we designed and synthesized H_2N-(RGD)$_4$, which possesses the same stereochemical RGD peptide arrangement as in ^{99m}Tc-(RGD)$_4$ and has a free amine suitable for labeling reactions. We radiolabeled H_2N-(RGD)$_4$ with ^{125}I and ^{211}At and obtained ^{125}I-(RGD)$_4$ and ^{211}At-(RGD)$_4$ with high radiochemical purity. As expected, ^{125}I-(RGD)$_4$ simultaneously bound to multiple integrin αvβ3 receptors in vitro and displayed high and persistent tumor uptake in vivo. In addition, the biodistribution study of ^{211}At-(RGD)$_4$ in tumor-bearing mice indicated that its biodistribution pattern was almost identical to that of ^{125}I-(RGD)$_4$, with no sign of in vivo deastatination. Though its high kidney uptake needs to be addressed by

combining other drug designs or strategies, ^{211}At-(RGD)$_4$ might be a potential radioligand for integrin αvβ3-targeted radionuclide therapy. These findings would be a useful basis for the development of novel integrin αvβ3-targeted drugs, in which high and persistent tumor uptake is a critical factor for therapeutic efficacy.

Experimental section

Materials and methods. L1, [11] H-(pG)$_6$-c[R(Pbf)GD(tBu)fK] (**20**), [11] *fac*-[Re^{I}(CO)$_3$(OH$_2$)$_3$]Br (**1**), [47] CN-OMe (**13**), [12] CN-GABA-TFP (**23**), [13] Re-(RGD)$_6$, [11] and ^{99m}Tc-(RGD)$_6$[11] were synthesized according to the method previously reported. [^{99m}Tc]TcO$_4^-$ was eluted in saline solution on daily basis from a ^{99}Mo/^{99m}Tc generator (PDRadiopharma Inc., Japan). [^{125}]NaI (643.8 GBq/mg) in 10 μM NaOH was obtained from PerkinElmer (USA). ^{211}At was produced by ^{209}Bi(α, 2n)^{211}At nuclear reaction using CYPRIS MP-30 cyclotron (Sumitomo Heavy Industries, Ltd., Japan) in the Advanced Clinical Research Center at Fukushima Medical University. [48] Radioactivity was measured by a dose calibrator (CRC-15R, Capintec Inc., USA) or an autowell gamma counter (WIZARD 1480, PerkinElmer Japan Co., Ltd., Japan). Mass spectrometry was performed on a solarix XR (Bruker Daltonics, Germany). ^{1}H NMR spectra were recorded on a JEOL ECZ-400S spectrometer (JEOL Ltd, Japan). IR spectra were recorded on a FT/IR-4700 (Jasco Co., Japan). All compounds are >95% pure by HPLC analysis.

CN-OH (2). To the solution of CN-OMe (**13**) (80.6 mg, 0.500 mmol) in 4 mL of MeOH was added 1 mL of 1 M NaOH. The reaction solution was stirred at room temperature for 2 h. After removing MeOH *in vacuo*, the solution was neutralized with 1 M HCl. This stock solution was used for following reactions without purification.

***cis*-[Re^{I}(CO)$_2$(CN-OH)$_4$]Cl (3).** To the solution of *fac*-[Re^{I}(CO)$_3$(OH$_2$)$_3$]Br (**1**) (4.12 mg, 10.2 μmol) in 10 mL of 0.1 M P.B. pH 8.0 was added 400 μL of CN-OH (**2**) stock solution (100 μmol). The reaction solution was heated at 100℃ for 30 min. After cooling, the reaction solution was applied to an Inert-Sep RP-C18 cartridge (GL Sciences Inc., Japan). The cartridge was washed with 20 mL of water to remove excess P.B. Then, compound **3** was eluted from the cartridge with 10 mL of MeOH. After removing MeOH *in vacuo*, the residue was purified with a semi-preparative HPLC (system 5). After HPLC purification, the solvent was removed *in vacuo*, and the residue was redissolved in the mixture of 5 mL of MeOH and 20 mL of 0.01 M HCl. The solution was applied to an Inert-Sep RP-C18 cartridge, and the cartridge was washed with 10 mL of 0.01 M HCl, followed by 10 mL of water. Compound **3** was eluted from the cartridge with 10 mL of MeOH. After removing MeOH *in vacuo*, the residue was dissolved in the mixture of acetonitrile and 0.01 M HCl. After lyophilization, compound **3** was obtained as a white solid (1.83 mg, 2.11 μmol, 20%). ESI-MS: calcd for $C_{34}H_{20}N_4O_{10}Re$, 831.07331; found, 831.07842 $[M]^+$. IR (ATR, ν/cm^{-1}): 2208.095 (m, CN), 2125.171 (br, CN), 2006.570 (s, CO), 1962.215 (s, CO).

***cis*-[Re^{I}(CO)$_2$(L1)$_4$]CF$_3$CO$_2$ (5).** *cis*-[Re^{I}(CO)$_2$(CN-OH)$_4$]Cl (**3**) (0.44 mg, 0.51 μmol), HCl·H-pG$_6$-c[R(pbf)GD(tBu)fK] (**20**) (4.72 mg, 2.52 μmol), HATU (1.65 mg, 4.33 μmol), and DIPEA (0.90 μL, 5.0 μmol) were dissolved in the mixture of 112.5 μL of acetonitrile and 22.5 μL of DMF. The reaction mixture was stirred at room temperature for 3 h and purified with a semi-preparative HPLC (system 6). After removing the solvent *in vacuo*, the residue was dissolved in TFA/TIS/Water (1.8/0.1/0.1 mL). The solution was stirred at

room temperature for 1 h, and the solvent was removed *in vacuo*. The residue was purified with a semi-preparative HPLC (system 5). After lyophilization, compound **5** was obtained as a white solid (0.65 mg, 0.0875 μmol, 17%). ESI-MS: calcd for $C_{310}H_{418}N_{88}O_{82}Na_3Re$, 1157.34258; found, 1157.33545 $[M+2H+3Na]^{6+}$.

***fac*-[Re^{I}(CO)$_3$(CN-OH)$_3$]Cl (6).** To the solution of *fac*-[Re^{I}(CO)$_3$(OH$_2$)$_3$]Br (**1**) (20.4 mg, 50.4 μmol) in 25 mL of 0.1 M A.B. pH 6.0 was added 1.2 mL of CN-OH (**2**) stock solution (300 μmol). The reaction solution was heated at 100°C for 3 h. After cooling, the reaction mixture was purified with a semi-preparative HPLC (system 5). After HPLC purification, compound **6** was converted to chloride salt using an Inert-Sep RP-C18 cartridge as described elsewhere. The appearance of compound **6** was a white solid (25.1 mg, 33.6 μmol, 67%). ESI-MS: calcd for $C_{27}H_{15}N_3O_9Re$, 712.03614; found, 712.05188 $[M]^+$. IR (ATR, ν/cm^{-1}): 2216.773 (m, CN), 2172.418 (s, CN), 2055.746 (s, CO), 1988.249 (s, CO).

***fac*-[Re^{I}(CO)$_3$(CN-OH)$_2$(CN-Et-NH-Boc)]Cl (7).** *fac*-[Re^{I}(CO)$_3$(CN-OH)$_3$]Cl (**6**) (8.90 mg, 11.9 μmol) was dissolved in 345 μL of DMF. To the solution was slowly added WSCD·HCl (2.28 mg, 11.9 μmol), N-Boc-1,2-diaminoethane (1.91 mg, 11.9 μmol), and HOBt·H$_2$O (3.64 mg, 23.8 μmol) dissolved in 250 μL of DMF. The reaction mixture was stirred at room temperature for 1 h and purified with a semi-preparative HPLC (system 7). After HPLC purification, compound **7** was converted to chloride salt using an Inert-Sep RP-C18 cartridge as described elsewhere. The appearance of compound **7** was a white solid (2.68 mg, 3.01 μmol, 25%). ESI-MS: calcd for $C_{34}H_{29}N_5O_{10}Re$, 854.14664; found, 854.17079 $[M]^+$.

***fac*-[Re^{I}(CO)$_3$(CN-pG$_6$-c(RGDfK))$_2$(CN-Et-NH$_2$)]Cl (9).** *fac*-[Re^{I}(CO)$_3$(CN-OH)$_2$(CN-Et-NH-Boc)]Cl (**7**) (3.65 mg, 4.11 μmol), HCl·H-pG$_6$-c[R(pbf)GD(tBu)fK] (**20**) (15.4 mg, 8.22 μmol), WSCD·HCl (2.36 mg, 12.3 μmol), HOBt·H$_2$O (1.89 mg, 12.3 μmol), and DIPEA (2.14 μL, 12.3 μmol) were dissolved in 205 μL of DMF. The reaction mixture was stirred at room temperature for 1.5 h and purified with a semi-preparative HPLC (system 8). After removing the solvent *in vacuo*, the residue was dissolved in TFA/TIS/Water (1.8/0.1/0.1 mL). The solution was stirred at room temperature for 1 h, and the solvent was removed *in vacuo*. The residue was purified with a semi-preparative HPLC (system 9). After HPLC purification, compound **9** was converted to hydrochloride salt using an Inert-Sep RP-C18 cartridge as described elsewhere. The appearance of compound **9** was a white solid (2.45 mg, 0.625 μmol, 15%). ESI-MS: calcd for $C_{167}H_{222}N_{47}O_{44}Re$, 944.40379; found, 944.44502 $[M+3H]^{4+}$.

***fac*-[Re^{I}(CO)$_3$(CN-OH)$_2$(CN-Et-NH-IB)]Cl (10).** *fac*-[Re^{I}(CO)$_3$(CN-OH)$_3$]Cl (**6**) (7.57 mg, 10.1 μmol) was dissolved in 258 μL of DMF. To the solution was added WSCD·HCl (1.94 mg, 10.1 μmol), H$_2$N-Et-NH-IB·HCl (**22**) (3.31 mg, 10.1 μmol), and HOBt·H$_2$O (3.10 mg, 20.3 μmol) dissolved in 249 μL of DMF. Lastly, DIPEA (4.66 μL, 26.8 μmol) was slowly added to the solution. The reaction mixture was stirred at room temperature for 1 h and purified with a semi-preparative HPLC (system 7). After HPLC purification, compound **10** was converted to chloride salt using an Inert-Sep RP-C18 cartridge as described elsewhere. The appearance of compound **10** was a white solid (1.27 mg, 1.25 μmol, 12%). ESI-MS: calcd for $C_{36}H_{24}IN_5O_9Re$, 984.01762; found, 984.01744 $[M]^{+}$.

^{nat}I-(RGD)$_2$ (12). *fac*-[Re^{I}(CO)$_3$(CN-OH)$_2$(CN-Et-NH-IB)]Cl (**10**) (0.96 mg, 0.94 μmol),

HCl·H-pG$_6$-c[R(pbf)GD(tBu)fK] (**20**) (3.53 mg, 1.88 μmol), WSCD·HCl (0.54 mg, 2.8 μmol), HOBt·H_2O (0.43 mg, 2.8 μmol), and DIPEA (0.49 μL, 2.8 μmol) were dissolved in 47 μL of DMF. The reaction mixture was stirred at room temperature for 2 h and purified with a semi-preparative HPLC (system 8). After removing the solvent *in vacuo*, the residue was dissolved in TFA/TIS/Water (1.8/0.1/0.1 mL). The reaction mixture was stirred at room temperature for 1 h and purified with a semi-preparative HPLC (system 10). After lyophilization, compound **12** was obtained as a white solid (1.55 mg, 0.357 μmol, 38%). ESI-MS: calcd for $C_{174}H_{224}IN_{47}O_{45}NaRe$, 1007.38001; found, 1007.38023 $[M+2H+Na]^{4+}$.

[Re^{I}(CN-OMe)$_4$(CO)Br] (14). [Re(CO)$_5$Br] (47.5 mg, 0.117 mmol) and CN-OMe (**13**) (95.0 mg, 0.589 mmol) were dissolved in 9.6 mL of toluene, and the mixture was heated at 100 ℃ for 14 h. After the solvent was removed *in vacuo*, the residue was purified by a preparative TLC (hexane/ethyl acetate = 1/1) (Merck KGaA, Germany) to afford compound **14** as a pale yellow solid (14.6 mg, 15.6 μmol, 13%). The ^{1}H NMR indicated the mixture of *cis*-[Re^{I}(CN-OMe)$_4$(CO)Br] (**14a**) and *trans*-[Re^{I}(CN-OMe)$_4$(CO)Br] (**14b**) (Figure S12). These two isomers were not separated at this step and used as a mixture in the next reaction. ESI-MS: calcd for $C_{37}H_{28}N_4O_9NaRe$, 961.04735; found, 961.05124 $[M+Na]^+$.

***cis*-[Re^{I}(CN-OMe)$_4$(CO)(CN-GABA-Et-NH-Boc)]CF$_3$CO$_2$ (15a).** To the solution of [Re^{I}(CN-OMe)$_4$(CO)Br] (**14**) (5.2 mg, 5.5 μmol) in 1 mL of chloroform was added $AgPF_6$ (3.2 mg, 13 μmol) dissolved in 0.2 mL of MeOH. A yellow precipitate was immediately formed and removed from the reaction mixture with a paper filter. To the filtrate was

added CN-GABA-Et-NH-Boc (**25**) (4.9 mg, 19 μmol) dissolved in 0.2 mL of MeOH. Then, 0.5 mL of toluene was added to the reaction solution, and the mixture was heated at 100°C for 1.5 h. After heating, the solvent was removed *in vacuo*, and the residue was purified with a semi-preparative HPLC (system 14). After lyophilization, compound **15a** was obtained as a white solid (1.97 mg, 1.61 μmol, 29%). ^{1}H NMR (Figure S13) (400 MHz, $CDCl_3$): δ 1.402 (s, 9H, *t*Bu), 2.187 (quint, 2H, CH_2), 2.510 (t, 2H, CH_2), 3.238 (br, 2H, CH_2), 3.310 (br, 2H, CH_2), 3.950 (s, 6H, OCH_3), 3.955 (s, 6H, OCH_3), 4.001 (t, 2H, CH_2), 7.524–8.163 (m, 16H, H_{arom}). ESI-MS: calcd for $C_{49}H_{49}N_7O_{12}Re$, 1114.29943; found 1114.31365 $[M]^+$.

***trans*-[Re^I(CN-OMe)$_4$(CO)(CN-GABA-Et-NH-Boc)]CF_3CO_2 (15b).** Compound **15b** was also isolated from the above reaction with a semi-preparative HPLC (system 14). After lyophilization, compound **15b** was obtained as a white solid (0.50 mg, 0.41 μmol, 7%). ^{1}H NMR (Figure S14) (400 MHz, $CDCl_3$): δ 1.393 (s, 9H, *t*Bu), 2.221 (quint, 2H, CH_2), 2.495 (t, 2H, CH_2), 3.227 (br, 2H, CH_2), 3.308 (br, 2H, CH_2), 3.955 (s, 12H, OCH_3), 4.001 (t, 2H, CH_2), 7.557–8.100 (m, 16H, H_{arom}). ESI-MS: calcd for $C_{49}H_{49}N_7O_{12}Re$, 1114.29943; found 1114.29499 $[M]^+$.

***cis*-[Re^I(CN-OH)$_4$(CO)(CN-GABA-Et-NH-Boc)]CF_3CO_2 (16).** *cis*-[Re^I(CN-OMe)$_4$(CO)(CN-GABA-Et-NH-Boc)]CF_3CO_2 (**15**) (1.35 mg, 1.10 μmol) was dissolved in 400 μL of MeOH. To the solution was added 100 μL of 1 M NaOH, and the reaction mixture was stirred at room temperature for 2 h. After the solution was neutralized with 1 M HCl, the crude compounds were purified with a semipreparative HPLC (system 15). After lyophilization, compound 16 was obtained as a white solid (1.27 mg, 1.08 μmol,

quant.). ^{1}H NMR (400 MHz, DMSO-d_6): δ 1.991 (quint, 2H, CH_2), 2.240 (t, 2H, CH_2), 2.928 (q, 2H, CH_2), 3.018 (q, 2H, CH_2), 4.004 (t, 2H, CH_2), 7.624–8.232 (m, 16H, H_{arom}). ESI-MS: calcd for $C_{45}H_{41}N_7O_{12}Re$, 1058.23707; found, 1058.23538 $[M]^+$.

***cis*-[Re^{I}(CN-pG$_6$-c(RGDfK))$_4$(CO)(CN-GABA-Et-NH$_2$)]CF$_3$CO$_2$ (18).** *cis*-[Re^{I}(CN-OH)$_4$(CO)(CN-GABA-Et-NH-Boc)]CF_3CO_2 (**16**) (1.0 mg, 0.85 μmol), HCl·H-pG$_6$-c[R(pbf)GD(tBu)fK] (**20**) (9.6 mg, 5.1 μmol), HATU (2.6 mg, 6.8 μmol), and DIPEA (1.8 μL, 10 μmol) were dissolved in 85 μL of DMF. The reaction mixture was stirred at room temperature for 2 h and purified with a semi-preparative HPLC (system 12). After removing the solvent *in vacuo*, the residue was dissolved in TFA/TIS/Water (1.8/0.1/0.1 mL). The solution was stirred at room temperature for 1 h, and the solvent was removed *in vacuo*. The residue was washed with diethyl ether and dissolved in water. After lyophilization, compound **18** was obtained as a white solid (4.4 mg, 0.57 μmol, 67%). ESI-MS: calcd for $C_{316}H_{433}N_{91}O_{82}NaRe$, 1171.36840; found, 1171.37539 $[M+4H+Na]^{6+}$.

***cis*-[Re^{I}(CN-pG$_6$-c(RGDfK))$_4$(CO)(CN-GABA-Et-NH-IB)]CF$_3$CO$_2$ (19).** *cis*-[Re^{I}(CN-pG$_6$-c(RGDfK))$_4$(CO)(CN-GABA-Et-NH$_2$)]CF_3CO_2 (**18**) (1.34 mg, 0.174 μmol), [^{nat}I]SIB (**25**) (0.12 mg, 0.35 μmol), HOBt·H_2O (0.05 mg, 0.3 μmol), and DIPEA (0.18 μL, 1.0 μmol) were dissolved in DMF. The reaction mixture was stirred at room temperature for 10 h and purified with a semi-preparative HPLC (system 13). After lyophilization, compound **19** was obtained as a white solid (1.0 mg, 0.13 μmol, 74%). ESI-MS: calcd for $C_{323}H_{436}IN_{91}O_{83}NaRe$, 1209.52091; found, 1209.52465 $[M+4H+Na]^{6+}$.

Boc-Et-NH-IB (21). 3-Iodobenzoic acid (138.3 mg, 0.5575 mmol), N-Boc-1,2-diaminoethane (89.3 mg, 0.557 mmol), and WSCD·HCl (213.9 mg, 1.116 mmol) were dissolved in 5.5 mL of chloroform. The reaction mixture was stirred at room temperature for 2 h. Then, the reaction solution was transferred to a separatory funnel and washed with 10 w/w% citric acid solution. The organic layer was collected and dried over anhydrous magnesium sulfate. The solvent was removed *in vacuo* to afford compound **21** as a yellow solid (140 mg, 0.359 mmol, 64%). ^{1}H NMR (400 MHz, $CDCl_3$): δ 1.447 (s, 9H, *t*Bu), 3.413 (q, 2H, C*H*$_2$), 3.543 (q, 2H, C*H*$_2$), 5.001 (br, 1H, N*H*), 7.346 (br, 1H, N*H*), 7.142-8.173 (m, 4H, *H*$_{arom}$). ESI-MS: calcd for $C_{14}H_{19}IN_2O_3Na$, 413.03326; found, 413.03328 $[M+Na]^+$.

H_2N-Et-NH-IB·HCl (22). Boc-Et-NH-IB (**21**) (134.0 mg, 0.3434 mmol) was dissolved in 5 mL of 4 M HCl/1,4-dioxane. After 30 min, the formed precipitate was collected and washed with diethyl ether. The precipitate was dried in vacuo to afford compound **22** as a white solid (99.6 mg, 0.305 mmol, 89%). ^{1}H NMR (400 MHz, DMSO-*d*$_6$): δ 2.9775 (m, 2H, C*H*$_2$), 3.5005 (q, 2H, C*H*$_2$), 7.293 (t, 1H, *H*$_{arom}$), 7.8965 (m, 1H, *H*$_{arom}$), 7.916 (m, 1H, *H*$_{arom}$), 7.976 (br, 2H, N*H*$_2$), 8.243 (t, 1H, *H*$_{arom}$), 8.799 (t, 1H, N*H*). ESI-MS: calcd for $C_9H_{12}IN_2O$, 290.99889; found, 290.99864 $[M+H]^+$.

CN-GABA-Et-NH-Boc (24). CN-GABA-TFP (**23**) (261 mg, 0.999 mmol) and N-Boc-1,2-diaminoethane (192 mg, 1.20 mmol) were dissolved in 10 mL of DMF. To the solution was added $NaHCO_3$ (420 mg, 5.00 mmol), and the reaction mixture was stirred at room temperature for 1 h. After NaHCO3 was removed with a paper filter, the solvent was removed *in vacuo*. The residue was dissolved in ethyl acetate and transferred to a

separatory funnel. The organic layer was washed with brine, collected, and dried over anhydrous magnesium sulfate. After the solvent was removed *in vacuo*, the residue was purified by silica gel chromatography (hexane/ethyl acetate = 1/4) to afford compound **24** as a white solid (89.1 mg, 0.349 mmol, 35%). ^{1}H NMR (400 MHz, $CDCl_3$): δ 1.450 (s, 9H, *t*Bu), 1.599 (s, 2H, C*H*$_2$), 1.976-2.056 (m, 2H, C*H*$_2$), 2.363 (t, 2H, C*H*$_2$), 3.285 (q, 2H, C*H*$_2$), 3.350-3.390 (m, 2H, C*H*$_2$), 3.474-3.516 (m, 2H, C*H*$_2$), 4.876 (br, 1H, N*H*), 6.303 (br, 1H, N*H*). ESI-MS: calcd for $C_{12}H_{21}N_3O_3Na$, 278.14751; found, 278.14926 $[M+Na]^+$.

[^{nat}I]SIB (25). 3-Iodobenzoic acid (248.0 mg, 1.00 mmol), N-hydroxysuccinimide (115.1 mg, 1.00 mmol), and WSCD·HCl (287.6 mg, 1.50 mmol) were dissolved in 3.3 mL of dichloromethane. The reaction mixture was stirred at room temperature for 1 h. The reaction solution was transferred to a separatory funnel and washed with 10 w/w% citric acid solution. The organic layer was collected and dried over anhydrous magnesium sulfate. The solvent was removed *in vacuo* to afford compound **25** as a white solid (279 mg, 0.808 mmol, 81%). ^{1}H NMR (400 MHz, CDCl3): δ 2.91 (s, 4H), 7.24-8.47 (m, 4H, H_{arom}).

Preparation of *fac*-[^{99m}Tc][Tc^{I}(CO)$_3$(OH$_2$)$_3$]$^+$.

fac-[^{99m}Tc][Tc^{I}(CO)$_3$(OH$_2$)$_3$]$^+$ was prepared according to the method previously reported[49] with slight modifications. To a 3 mL glass vial containing 5.5 mg of $NaBH_4$, 4.0 mg of Na_2CO_3, and 10 mg of Sodium (+)-tartrate dihydrate was added 500 μL of freshly eluted [^{99m}Tc][TcO_4]$^-$ (≈ 150 MBq). The vial was then purged with 50 mL of CO, followed by heating at 85°C for 15 min. After cooling to room temperature, the pH of the

solution was adjusted to around 5 with 1 M HCl. The radiochemical purity was determined by HPLC (system 1). *fac*-[^{99m}Tc][Tc^{I}(CO)$_3$(OH$_2$)$_3$]$^+$ was used for the following reaction without purification.

Preparation of ^{99m}Tc-(RGD)$_4$

L1 (120 nmol) was dissolved in 180 μL of 0.2 M MES buffer (pH 5.0) and mixed with 120 μL of freshly prepared *fac*-[^{99m}Tc][Tc^{I}(CO)$_3$(OH$_2$)$_3$]$^+$ (≈ 30 MBq). To prevent non-specific absorption, 1.5 μL of 10% v/v Tween 20 was added. The reaction vessel was purged with N_2 and heated at 95°C for 30 min. After cooling to room temperature, the reaction solution was purified by HPLC (system 2). The fraction of HPLC eluent containing ^{99m}Tc-(RGD)$_4$ was collected, and methanol was removed by rotary evaporation. A solution of 10% Tween-20 was added to the purified ^{99m}Tc-(RGD)$_4$, resulting in a final Tween-20 concentration of 0.1 %. The radiochemical purity was determined by HPLC (system 2). The radiochemical yield without decay correction was calculated by dividing the radioactivity of purified ^{99m}Tc-(RGD)$_4$ by the radioactivity of *fac*-[^{99m}Tc][Tc^{I}(CO)$_3$(OH$_2$)$_3$]$^+$ used for the reaction.

Preparation of [^{125}I]SIB

[^{125}I]SIB was prepared according to the method previously reported[50] with slight modifications. A solution of 144.4 mg of STB (Toronto Research Chemicals Inc., Canada) in 72.2 μL of 5% acetic acid/MeOH and a solution of 40 μg of NCS in 20 μL of MeOH were prepared. These solutions were added to a reaction vessel containing [^{125}I]NaI (≈ 15 MBq), and the reaction solution was left at room temperature for 30 min. The reaction

solution was diluted with 138 μL of 5%AcOH/water and purified by HPLC (system 4). The fraction containing [^{125}I]SIB was collected and diluted with 3 mL of 5%AcOH/water. The purified solution was applied to a Sep-Pak C18 cartridge (Waters, USA), and the cartridge was washed with 5 mL of water. After the cartridge was purged with air, [^{125}I]SIB was eluted from the cartridge with acetonitrile. The eluent was collected in fractions of 100 μL each, and the fraction containing the highest radioactivity was used for the following reactions. The radiochemical yields were ≈ 80%.

Preparation of [^{211}At]SAB

A similar method was employed in the preparation of [^{211}At]SAB as was used for [^{125}I]SIB. ^{211}At was isolated by a dry distillation method and supplied dissolved in chloroform. A solution of ^{211}At (3.4 MBq)/chloroform was prepared in a reaction vial, and chloroform was removed by a stream of N_2. A solution of 144.4 mg of STB in 72.2 μL of 5% acetic acid/MeOH and a solution of 40 μg of NCS in 20 μL of MeOH were added to the vial. The reaction solution was left at room temperature for 30 min. [^{211}At]SAB was purified using the same method employed for [^{125}I]SIB. The radiochemical yield without decay correction was 66%.

Preparation of ^{125}I-(RGD)$_2$

A solution of [^{125}I]SIB (≈ 6 MBq)/acetonitrile was prepared in a reaction vial, and acetonitrile was removed by a stream of air using a Smart Evaporator (BioChromato, Inc., Japan). To this reaction vial was added 10 nmol of compound **6** dissolved in 10 μL of 0.1 M borate buffer (pH 9.0). The reaction solution was left at room temperature for 3 h and purified by HPLC (system 3). The fraction containing ^{125}I-(RGD)$_2$ was collected, and the

HPLC solvent was removed by rotary evaporation. ^{125}I-(RGD)$_2$ was reconstituted in saline containing 0.1% Tween-20. The radiochemical purity was determined by HPLC (system 3). The radiochemical yield was calculated by dividing the radioactivity of purified ^{125}I-(RGD)$_2$ by the radioactivity of [^{125}I]SIB used for the reaction.

Preparation of ^{125}I-(RGD)$_4$

A similar method was employed in the preparation of ^{125}I-(RGD)$_4$ as was used for ^{125}I-(RGD)$_2$. A solution of [^{125}I]SIB (≈ 6 MBq)/acetonitrile was prepared in a reaction vial, and acetonitrile was removed by stream of air using a Smart Evaporator. To this reaction vial was added 10 nmol of H_2N-(RGD)$_4$ (**18**) dissolved in 10 μL of 0.1 M borate buffer (pH 9.0). The reaction solution was left at room temperature for 3 h and purified by HPLC (system 3). The fraction containing ^{125}I-(RGD)$_4$ was collected, and the HPLC solvent was removed by rotary evaporation. ^{125}I-(RGD)$_4$ was reconstituted in saline containing 0.1% Tween-20. The radiochemical purity was determined by HPLC (system 3). The radiochemical yield was calculated by dividing the radioactivity of purified ^{125}I-(RGD)$_4$ by the radioactivity of [^{125}I]SIB used for the reaction.

Preparation of ^{211}At-(RGD)$_4$

A solution of [^{211}At]SAB (≈ 2 MBq)/acetonitrile was prepared in a reaction vial, and acetonitrile was removed by a rotary evaporator. To this reaction vial was added 20 nmol of H_2N-(RGD)$_4$ (**18**) dissolved in 10 μL of 0.1 M borate buffer (pH 9.0). The reaction solution was left at room temperature for 30 min and purified by HPLC (system 3). The fraction containing ^{211}At-(RGD)$_4$ was collected, and the HPLC solvent was removed by rotary evaporation. ^{211}At-(RGD)$_4$ was reconstituted in saline containing 0.1% Tween-20.

The radiochemical purity was determined by HPLC (system 3). The radiochemical yield was calculated by dividing the radioactivity of purified ^{211}At-(RGD)$_4$ by the radioactivity of [^{211}At]SAB used for the reaction.

In vitro stability of ^{125}I-(RGD)$_4$.

This experiment was performed according to the method we previously reported[13], and detailed methods are presented in the Supporting Information.

In vitro binding affinity to integrin αvβ3 / Cellular uptake and dissociation study / Dissociation kinetics in the presence of c(RGDyV)

These experiments were performed according to the method we previously reported[11], and detailed methods are presented in the Supporting Information.

Kinetic analysis of the dissociation data

The dissociation rate constants (k_{off}) of ^{125}I-(RGD)$_2$, ^{125}I-(RGD)$_4$, ^{99m}Tc-(RGD)$_6$, and ^{99m}Tc-(RGD)$_4$ were determined by fitting the dissociation data shown in Figure 4 to a non-linear one-phase exponential decay model using GraphPad Prism v. 9.

Animal model

All animal experiments were performed following the Act on Welfare and Management of Animals and were approved by the Institutional Animal Care and Use Committee of National University Corporation Hokkaido University (approval no. 19-0150 and 24-0050). Five-week-old BALBc nu/nu male mice (Japan SLC, Inc., Japan) were xenografted by subcutaneous injection of MDA-MB-435S cells (5×10^6 cells per 50 μL

of culture medium) into their right shoulders. Two weeks after MDA-MB-435S cell inoculation, the same mice were xenografted by subcutaneous injection of U87MG cells (5×10^6 cells per 50 μL of culture medium) into their left shoulders. Three weeks after U87MG cell inoculation, the mice were subjected to biodistribution studies.

Biodistribution of ^{99m}Tc-(RGD)$_6$, ^{99m}Tc-(RGD)$_4$, ^{125}I-(RGD)$_4$, and ^{125}I-(RGD)$_2$.

BALB/c nu/nu male mice bearing both U87MG and MDA-MB-435S tumors were injected via the tail vein with 100 μL of either the mixture of 10 kBq ^{125}I-(RGD)$_2$ and 100 kBq ^{99m}Tc-(RGD)$_6$ or the mixture of 10 kBq ^{125}I-(RGD)$_4$ and 100 kBq ^{99m}Tc-(RGD)$_4$. For the blocking experiments, 500 nmol of c(RGDyV) was coinjected. The mice were sacrificed and dissected at 1, 4, and 24 h after administration. The tissues of interest were removed and weighed, and the radioactivity of ^{125}I and ^{99m}Tc was simultaneously measured by a dual isotope counting method with spillover correction using an autowell gamma counter. As a counting window for ^{125}I, dynamic-% with the peak position of 29 keV and the window coverage of 97% was employed. As a counting window for ^{99m}Tc, dynamic-% with the peak position of 140 keV and the window coverage of 90% was employed. We have confirmed no radioactivity spillover between ^{125}I and ^{99m}Tc under this condition. The results are presented as percent injected dose per gram (%ID/g) with values expressed as mean ± SD for a group of 4, 5, or 6 animals.

Biodistribution of ^{211}At-(RGD)$_4$ and ^{125}I-(RGD)$_4$.

BALB/c nu/nu male mice bearing U87MG tumor were injected via the tail vein with 100 μL of the mixture of 15 kBq ^{211}At-(RGD)$_4$ and 5 kBq ^{125}I-(RGD)$_4$. For the blocking experiments, 500 nmol of c(RGDfK) was coinjected. The mice were sacrificed and

dissected at 5 min, 1, 4, and 24 h after administration, and the tissues of interest were removed and weighed. Because it was technically challenging to isolate the thyroid, we collected the thyroid along with the trachea. The radioactivity of ^{211}At was measured by an autowell gamma counter with the fixed energy window of 61-111 keV. The spillover of ^{125}I radioactivity into this energy window was 0.12 and 0.06% when ^{125}I count was 162,576 and 30662 cpm, respectively, which is reasonably low to practically ignore the influence of the spillover. To avoid the spillover of ^{211}At radioactivity into the ^{125}I counting window described elsewhere, the samples were left for a week to ensure the decay of ^{211}At before the measurement of ^{125}I. To measure the radioactivity in the urine and feces collected over 24 h after the injection, each mouse was kept in a single cage with enough animal bedding. After 24 h, the animal bedding was manually separated from the feces, and the radioactivity in the animal bedding was regarded as the radioactivity excreted into the urine. No radioactivity remained in the singles cages. The results are presented as percent injected dose (%ID) or percent injected dose per gram (%ID/g) with values expressed as mean ± SD for a group of 3 or 4 animals.

Radiation dosimetry estimates of ^{211}At-(RGD)$_4$.

The radiation dosimetry estimates of ^{211}At-(RGD)$_4$ in a 25 g mouse phantom model was calculated using OLINDA/EXM 2.3.0 (HERMES Medical Solutions, Sweden). The values of %ID in organs of interest obtained from the biodistribution experiment were entered into OLINDA to calculate time-integrated activity coefficient (Bq-h/Bq). Then, radiation dosimetry estimates were calculated by multiplying the obtained time-integrated activity coefficients by dose conversion factors (mGy/MBq-s), a radionuclide and phantom model specific parameter. The calculation of radiation dosimetry estimate in the

U87MG tumor was performed using a sphere phantom model based on the assumption that all tumors had a mass of 0.1 g. Radiation dosimetry estimates using a sphere phantom model is generally sensitive to the size of the sphere. However, this is not the case for α-emitting radionuclides because of its short path-length.

Statistical analyses

Statistical significance was calculated using unpaired Student's t-tests, paired Student's t-tests, or extra sum of squares F test by GraphPad Prism 9.0 (GraphPad Software, Inc., USA) $*P < 0.05$.

Associated content

Supporting Information

The Supporting Information is available free of charge. HPLC methods, HPLC chromatograms, western blotting, ESI-MS spectrums, ^{1}H NMR spectrums, Biodistribution, supplementary methods.

Molecular formula strings

Author information

Corresponding Authors

Yuki Mizuno

Central Institute of Isotope Science, Hokkaido University, 060-0815, Japan

Global Center for Biomedical Science and Engineering, Hokkaido University, 060-8638, Japan

Email: mizuno@ric.hokudai.ac.jp

Authors

Thanakrit Suebboonprathueng

Graduate School of Biomedical Science and Engineering, Hokkaido University, Sapporo, Japan

Satoru Onoe

Laboratory of Physical Chemistry, Showa Pharmaceutical University, Machida, Japan

Hiromichi Akizawa

Laboratory of Physical Chemistry, Showa Pharmaceutical University, Machida, Japan

Ken-ichi Nishijima

Advanced Clinical Research Center, Fukushima Medical University, Fukushima, Japan

Kazuhiro Takahashi

Advanced Clinical Research Center, Fukushima Medical University, Fukushima, Japan

Yuji Kuge

Central Institute of Isotope Science, Hokkaido University, 060-0815, Japan

Global Center for Biomedical Science and Engineering, Hokkaido University, 060-8638, Japan

Author Contributions

Yuki Mizuno: Conceptualization, Data curation, Formal analysis, Funding acquisition, Investigation, Visualization, Writing – original draft. Thanakrit Suebboonprathueng: Investigation, Writing – review & editing. Satoru Onoe: Methodology, Validation, Writing – review & editing. Hiromichi Akizawa: Validation, Writing – review & editing.

Kenichi Nishijima: Resources, Validation, Writing – review & editing. Kazuhiro Takahashi: Resources, Validation, Writing – review & editing. Yuji Kuge: Validation, Writing – review & editing.

Notes

The authors declare no competing financial interest.

Acknowledgments

This work was supported by JSPS KAKENHI Grant Number 22H03007 and 23K24268. The authors thank Ms. Tamayo Hayashi for her excellent technical support in peptide synthesis, cell culture, and animal experiments.

■ Abbreviations

A.B., acetate buffer; BSA, bovine serum albumin; *t*Bu, *tert*-butyl; DIPEA, *N,N*-diisopropylethylamine; DMF, *N,N*-dimethylformamide; ESI-MS, electrospray ionization-mass spectrometry; HATU, 1-[bis(dimethylamino)methylene]-1*H*-1,2,3-triazolo[4,5-*b*]pyridinium 3-oxide hexafluorophosphate; HOBt·H_2O, 1-Hydroxybenzotriazole monohydrate; HPLC, high-performance liquid chromatography; IC_{50}, half maximal inhibitory concentration; MeOH, methanol; MES, 2-morpholinoethanesulfonic acid; NCS, N-Chlorosuccinimide; Pbf, 2,2,4,6,7-pentamethyldihydrobenzofuran-5-sulfonyl; P.B., phosphate buffer; PBS, phosphate buffered saline; p.i., post injection; SAB, *N*-succinimidyl 3-astatobenzoate; SD, standard deviation; SIB, *N*-succinimidyl 3-iodobenzoate; STB, *N*-succinimidyl 3-(tri-methylstannyl)benzoate; TFA, trifluoroacetic acid; TIS, triisopropylsilane; TLC, thin

layer chromatography; WSCD·HCl, 1-(3-dimethylaminopropyl)-3-ethylcarbodiimide hydrochloride.

■ References

(1) Lepareur, N.; Ramée, B.; Mougin-Degraef, M.; Bourgeois, M. Clinical Advances and Perspectives in Targeted Radionuclide Therapy. *Pharmaceutics* **2023**, *15* (6), 1733.
(2) Czerwińska, M.; Bilewicz, A.; Kruszewski, M.; Wegierek-Ciuk, A.; Lankoff, A. Targeted Radionuclide Therapy of Prostate Cancer—From Basic Research to Clinical Perspectives. *Molecules* **2020**, *25* (7), 1743.
(3) Hebert, K.; Santoro, L.; Monnier, M.; Castan, F.; Berkane, I.; Assénat, E.; Fersing, C.; Gélibert, P.; Pouget, J.-P.; Bardiès, M.; et al. Absorbed Dose–Response Relationship in Patients with Gastroenteropancreatic Neuroendocrine Tumors Treated with [^{177}Lu]Lu-DOTATATE: One Step Closer to Personalized Medicine. *J. Nucl. Med.* **2024**, *65* (6), 923-930.
(4) Böhmer, V. I.; Szymanski, W.; Feringa, B. L.; Elsinga, P. H. Multivalent Probes in Molecular Imaging: Reality or Future? *Trends Mol. Med.* **2021**, *27* (4), 379-393.
(5) Cossu, J.; Thoreau, F.; Boturyn, D. Multimeric RGD-Based Strategies for Selective Drug Delivery to Tumor Tissues. *Pharmaceutics* **2023**, *15* (2), 525.
(6) Liolios, C.; Sachpekidis, C.; Kolocouris, A.; Dimitrakopoulou-Strauss, A.; Bouziotis, P. PET Diagnostic Molecules Utilizing Multimeric Cyclic RGD Peptide Analogs for Imaging Integrin αvβ3 Receptors. *Molecules* **2021**, *26* (6), 1792.
(7) Kiessling, L. L.; Gestwicki, J. E.; Strong, L. E. Synthetic Multivalent Ligands as Probes of Signal Transduction. *Angew. Chem. Int. Ed.* **2006**, *45* (15), 2348-2368.
(8) Kiessling, L. L.; Gestwicki, J. E.; Strong, L. E. Synthetic Multivalent Ligands in the Exploration of Cell-Surface Interactions. *Curr. Opin. Chem. Biol.* **2000**, *4* (6), 696-703.
(9) Mammen, M.; Choi, S. K.; Whitesides, G. M. Polyvalent Interactions in Biological Systems: Implications for Design and Use of Multivalent Ligands and Inhibitors. *Angew. Chem. Int. Ed.* **1998**, *37* (20), 2754-2794.
(10) Vauquelin, G.; Charlton, S. J. Exploring Avidity: Understanding the Potential Gains in Functional Affinity and Target Residence Time of Bivalent and Heterobivalent Ligands. *Br. J. Pharmacol.* **2013**, *168* (8), 1771-1785.
(11) Mizuno, Y.; Kimura, K.; Onoe, S.; Shukuri, M.; Kuge, Y.; Akizawa, H. Influence of Linker Molecules in Hexavalent RGD Peptides on Their Multivalent Interactions with Integrin αvβ3. *J. Med. Chem.* **2021**, *64* (21), 16008-16019.
(12) Mizuno, Y.; Komatsu, N.; Uehara, T.; Shimoda, Y.; Kimura, K.; Arano, Y.; Akizawa, H. Aryl Isocyanide Derivative for One-pot Synthesis of Purification-Free ^{99m}Tc-Labeled Hexavalent Targeting Probe. *Nucl. Med. Biol.* **2020**, *86-87*, 30-36.
(13) Mizuno, Y.; Uehara, T.; Jen, C.-W.; Akizawa, H.; Arano, Y. The Synthesis of a ^{99m}Tc-

Labeled Tetravalent Targeting Probe upon Isonitrile Coordination to $^{99m}Tc^{I}$ for Enhanced Target Uptake in Saturable Systems. *RSC Advances* **2019**, *9* (45), 26126-26135.
(14) Echavidre, W.; Picco, V.; Faraggi, M.; Montemagno, C. Integrin-αvβ3 as a Therapeutic Target in Glioblastoma: Back to the Future? *Pharmaceutics* **2022**, *14* (5), 1053.
(15) Wu, J.; Tian, J.; Zhang, Y.; Ji, H.; Sun, J.; Wang, X.; Sun, C.; Wang, L.; Teng, Z.; Lu, G.; et al. ^{18}F-Alfatide II for the Evaluation of Axillary Lymph Nodes in Breast Cancer Patients: Comparison with ^{18}F-FDG. *Eur. J. Nucl. Med. Mol. Imaging* **2022**, *49* (8), 2869-2876.
(16) Carlsen, E. A.; Loft, M.; Loft, A.; Czyzewska, D.; Andreassen, M.; Langer, S. W.; Knigge, U.; Kjaer, A. Prospective Phase II Trial of [^{68}Ga]Ga-NODAGA-E[c(RGDyK)]$_2$ PET/CT Imaging of Integrin $\alpha_v\beta_3$ for Prognostication in Patients with Neuroendocrine Neoplasms. *J. Nucl. Med.* **2023**, *64* (2), 252-259.
(17) Cluzel, C.; Saltel, F.; Lussi, J.; Paulhe, F.; Imhof, B. A.; Wehrle-Haller, B. The Mechanisms and Dynamics of $\alpha_v\beta_3$ Integrin Clustering in Living Cells. *J. Cell Biol.* **2005**, *171* (2), 383-392.
(18) Kapp, T. G.; Rechenmacher, F.; Neubauer, S.; Maltsev, O. V.; Cavalcanti-Adam, E. A.; Zarka, R.; Reuning, U.; Notni, J.; Wester, H.-J.; Mas-Moruno, C.; et al. A Comprehensive Evaluation of the Activity and Selectivity Profile of Ligands for RGD-Binding Integrins. *Sci. Rep.* **2017**, *7*, 39805.
(19) Ballal, S.; Yadav, M. P.; Satapathy, S.; Raju, S.; Tripathi, M.; Damle, N. A.; Sahoo, R. K.; Bal, C. Long-term Survival Outcomes of Salvage [^{225}Ac]Ac-PSMA-617 Targeted Alpha Therapy in Patients with PSMA-expressing End-stage Metastatic Castration-resistant Prostate Cancer: A Real-World Study. *Eur. J. Nucl. Med. Mol. Imaging* **2023**, *50* (12), 3777-3789.
(20) Kratochwil, C.; Bruchertseifer, F.; Giesel, F. L.; Weis, M.; Verburg, F. A.; Mottaghy, F.; Kopka, K.; Apostolidis, C.; Haberkorn, U.; Morgenstern, A. ^{225}Ac-PSMA-617 for PSMA-Targeted α-Radiation Therapy of Metastatic Castration-Resistant Prostate Cancer. *J. Nucl. Med.* **2016**, *57* (12), 1941-1944.
(21) Kurz, P.; Spingler, B.; Fox, T.; Alberto, R. $[Tc^{1}(CN)_3(CO)_3]^{2-}$ and $[Re^{1}(CN)_3(CO)_3]^{2-}$: Case Studies for the Binding Properties of CN- and CO. *Inorg. Chem.* **2004**, *43* (13), 3789-3791.
(22) Chen, X.; Guo, Y.; Zhang, Q.; Hao, G.; Jia, H.; Liu, B. Preparation and Biological Evaluation of ^{99m}Tc-CO-MIBI as Myocardial Perfusion Imaging Agent. *J. Organomet. Chem.* **2008**, *693* (10), 1822-1828.
(23) Dyszlewski, M.; Blake, H. M.; Dahlheimer, J. L.; Pica, C. M.; Piwnica-Worms, D.

Characterization of a Novel ^{99m}Tc-Carbonyl Complex as a Functional Probe of MDR1 P-Glycoprotein Transport Activity. *Mol. Imaging* **2002**, *1* (1), 24-35.
(24) Ditri, T. B.; Fox, B. J.; Moore, C. E.; Rheingold, A. L.; Figueroa, J. S. Effective Control of Ligation and Geometric Isomerism: Direct Comparison of Steric Properties Associated with Bis-mesityl and Bis-diisopropylphenyl *m*-Terphenyl Isocyanides. *lnorg. Chem.* **2009**, *48* (17), 8362-8375.
(25) Xiangyun, W.; Yi, W.; Xinqi, L.; Taiwei, C.; Shaowen, H.; Xionghui, W.; Boli, L. The Structure, Energy and Stability of Components Formed in the Preparation of *fac*-[^{99m}Tc(CO)$_3$(H$_2$O)$_3$]$^+$. *Phys. Chem. Chem. Phys.* **2003**, *5* (3), 456-460.
(26) King, R. B.; Saran, M. S. Isocyanide-Metal Complexes. II. CO and CN Stretching Modes in *tert*-Butyl Isocyanide Derivatives of the Octahedral Metal Carbonyls. *lnorg. Chem.* **1974**, *13* (1), 74-78.
(27) Mizuno, Y.; Uehara, T.; Hanaoka, H.; Endo, Y.; Jen, C.-W.; Arano, Y. Purification-Free Method for Preparing Technetium-99m-Labeled Multivalent Probes for Enhanced in Vivo Imaging of Saturable Systems. *J. Med. Chem.* **2016**, *59* (7), 3331-3339.
(28) Claude, G.; Weh, D.; Hagenbach, A.; Figueroa, J. S.; Abram, U. Rhenium Complexes with p-Fluorophenylisocyanide. *Z. Anorg. Allg. Chem.* **2023**, *649* (1), e202200320.
(29) Stabin, M. G. OLINDA/EXM 2—The Next-Generation Personal Computer Software for Internal Dose Assessment in Nuclear Medicine. *Health Phys.* **2023**, *124* (5), 397-406.
(30) Bondza, S.; ten Broeke, T.; Nestor, M.; Leusen, J. H. W.; Buijs, J. Bivalent Binding on Cells Varies between Anti-CD20 Antibodies and is Dose-dependent. *mAbs* **2020**, *12* (1), 1792673.
(31) Ivan, T.; Enkvist, E.; Sinijarv, H.; Uri, A. Competitive Ligands Facilitate Dissociation of the Complex of Bifunctional Inhibitor and Protein Kinase. *Biophys. Chem.* **2017**, *228*, 17-24.
(32) Mack, E. T.; Snyder, P. W.; Perez-Castillejos, R.; Bilgiçer, B.; Moustakas, D. T.; Butte, M. J.; Whitesides, G. M. Dependence of Avidity on Linker Length for a Bivalent Ligand–Bivalent Receptor Model System. *J. Am. Chem. Soc.* **2012**, *134* (1), 333-345.
(33) Wilbur, D. S.; Thakar, M. S.; Hamlin, D. K.; Santos, E. B.; Chyan, M.-K.; Nakamae, H.; Pagel, J. M.; Press, O. W.; Sandmaier, B. M. Reagents for Astatination of Biomolecules. 4. Comparison of Maleimido-closo-Decaborate(2-) and meta-[^{211}At]Astatobenzoate Conjugates for Labeling anti-CD45 Antibodies with [^{211}At]Astatine. *Bioconjugate Chem.* **2009**, *20* (10), 1983-1991.
(34) Wilbur, D. S.; Chyan, M.-K.; Hamlin, D. K.; Kegley, B. B.; Risler, R.; Pathare, P. M.; Quinn, J.; Vessella, R. L.; Foulon, C.; Zalutsky, M.; et al. Reagents for Astatination of Biomolecules: Comparison of the in Vivo Distribution and Stability of Some

Radioiodinated/Astatinated Benzamidyl and *nido*-Carboranyl Compounds. *Bioconjugate Chem.* **2004**, *15* (1), 203-223.
(35) Hirata, S.; Mishiro, K.; Washiyama, K.; Munekane, M.; Fuchigami, T.; Arano, Y.; Takahashi, K.; Kinuya, S.; Ogawa, K. In Vivo Stability Improvement of Astatobenzene Derivatives by Introducing Neighboring Substituents. *J. Med. Chem.* **2025**, *68* (2), 1540-1552.
(36) Suzuki, H.; Kannaka, K.; Hirayama, M.; Yamashita, T.; Kaizuka, Y.; Kobayashi, R.; Yasuda, T.; Takahashi, K.; Uehara, T. In Vivo Stable ^{211}At-Labeled Prostate-Specific Membrane Antigen-Targeted Tracer Using a Neopentyl Glycol Structure. *EJNMMI Radiopharm. Chem.* **2024**, *9* (1), 48.
(37) Suzuki, H.; Kaizuka, Y.; Tatsuta, M.; Tanaka, H.; Washiya, N.; Shirakami, Y.; Ooe, K.; Toyoshima, A.; Watabe, T.; Teramoto, T.; et al. Neopentyl Glycol as a Scaffold to Provide Radiohalogenated Theranostic Pairs of High In Vivo Stability. *J. Med. Chem.* **2021**, *64* (21), 15846-15857.
(38) Li, Z.-b.; Cai, W.; Cao, Q.; Chen, K.; Wu, Z.; He, L.; Chen, X. ^{64}Cu-Labeled Tetrameric and Octameric RGD Peptides for Small-Animal PET of Tumor $\alpha_v\beta_3$ Integrin Expression. *J. Nucl. Med.* **2007**, *48* (7), 1162-1171.
(39) Akizawa, H.; Uehara, T.; Arano, Y. Renal Uptake and Metabolism of Radiopharmaceuticals Derived from Peptides and Proteins. *Adv. Drug Del. Rev.* **2008**, *60* (12), 1319-1328.
(40) Chen, X.; Sievers, E.; Hou, Y.; Park, R.; Tohme, M.; Bart, R.; Bremner, R.; Bading, J. R.; Conti, P. S. Integrin αvβ3-Targeted Imaging of Lung Cancer. *Neoplasia* **2005**, *7* (3), 271-279.
(41) Suzuki, H.; Araki, M.; Tatsugi, K.; Ichinohe, K.; Uehara, T.; Arano, Y. Reduction of the Renal Radioactivity of ^{111}In-DOTA-Labeled Antibody Fragments with a Linkage Cleaved by the Renal Brush Border Membrane Enzymes. *J. Med. Chem.* **2023**, *66* (13), 8600-8613.
(42) Suzuki, H.; Kise, S.; Kaizuka, Y.; Watanabe, R.; Sugawa, T.; Furukawa, T.; Fujii, H.; Uehara, T. Copper-64-Labeled Antibody Fragments for Immuno-PET/Radioimmunotherapy with Low Renal Radioactivity Levels and Amplified Tumor-Kidney Ratios. *ACS Omega* **2021**, *6* (33), 21556-21562.
(43) Arano, Y. Renal Brush Border Strategy: A Developing Procedure to Reduce Renal Radioactivity Levels of Radiolabeled Polypeptides. *Nucl. Med. Biol.* **2021**, *92*, 149-155.
(44) Jin, Z. H.; Furukawa, T.; Sogawa, C.; Claron, M.; Aung, W.; Tsuji, A. B.; Wakizaka, H.; Zhang, M. R.; Boturyn, D.; Dumy, P.; et al. PET Imaging and Biodistribution Analysis of the Effects of Succinylated Gelatin Combined with L-Lysine on Renal Uptake and

Retention of ^{64}Cu-cyclam-RAFT-c(-RGDfK-)$_4$ In Vivo. *Eur. J. Pharm. Biopharm.* **2014**, *86* (3), 478-486.
(45) Briat, A.; Wenk, C. H. F.; Ahmadi, M.; Claron, M.; Boturyn, D.; Josserand, V.; Dumy, P.; Fagret, D.; Coll, J.-L.; Ghezzi, C.; et al. Reduction of Renal Uptake of ^{111}In-DOTA-Labeled and A700-Labeled RAFT-RGD During Integrin αvβ3 Targeting using Single Photon Emission Computed Tomography and Optical Imaging. *Cancer Sci.* **2012**, *103* (6), 1105-1110.
(46) Stangl, S.; Nguyen, N. T.; Brosch-Lenz, J.; Šimeček, J.; Weber, W. A.; Kossatz, S.; Notni, J. Efficiency of Succinylated Gelatin and Amino Acid Infusions for Kidney Uptake Reduction of Radiolabeled αvβ6-Integrin Targeting Peptides: Considerations on Clinical Safety Profiles. *Eur. J. Nucl. Med. Mol. Imaging* **2024**, *51* (11), 3191-3201.
(47) Lazarova, N.; James, S.; Babich, J.; Zubieta, J. A Convenient Synthesis, Chemical Characterization and Reactivity of $[Re(CO)_3(H_2O)_3]Br$: The Crystal and Molecular Structure of $[Re(CO)_3(CH_3CN)_2Br]$. *Inorg. Chem. Commun.* **2004**, *7* (9), 1023-1026.
(48) Washiyama, K.; Oda, T.; Sasaki, S.; Aoki, M.; Guerra Gomez, F. L.; Taniguchi, M.; Nishijima, K.-i.; Takahashi, K. At-211 Production using the CYPRIS MP-30. *J. Med. Imaging Radiat. Sci.* **2019**, *50* (1), S42.
(49) Alberto, R.; Schibli, R.; Egli, A.; Schubiger, A. P.; Abram, U.; Kaden, T. A. A Novel Organometallic Aqua Complex of Technetium for the Labeling of Biomolecules: Synthesis of $[^{99m}Tc(OH_2)_3(CO)_3]^+$ from $[^{99m}TcO_4]^-$ in Aqueous Solution and Its Reaction with a Bifunctional Ligand. *J. Am. Chem. Soc.* **1998**, *120* (31), 7987-7988.
(50) Aoki, M.; Zhao, S.; Takahashi, K.; Washiyama, K.; Ukon, N.; Tan, C.; Shimoyama, S.; Nishijima, K.-i.; Ogawa, K. Preliminary Evaluation of Astatine-211-Labeled Bombesin Derivatives for Targeted Alpha Therapy. *Chem. Pharm. Bull.* **2020**, *68* (6), 538-545.

Table of Contents Graphic